J Physiol 0.0 (2023) pp 1–22

The Journal of Physiology

A detailed analysis of single-channel $Na_v1.5$ recordings does not reveal any cooperative gating

Zoja Selimi[1], Jean-Sébastien Rougier[2], Hugues Abriel[2] and Jan P. Kucera[1]

[1]*Department of Physiology, University of Bern, Bern, Switzerland*
[2]*Institute of Biochemistry and Molecular Medicine, University of Bern, Bern, Switzerland*

Handling Editors: Bjorn Knollmann & Brian Delisle

The peer review history is available in the Supporting Information section of this article (https://doi.org/10.1113/JP284861#support-information-section).

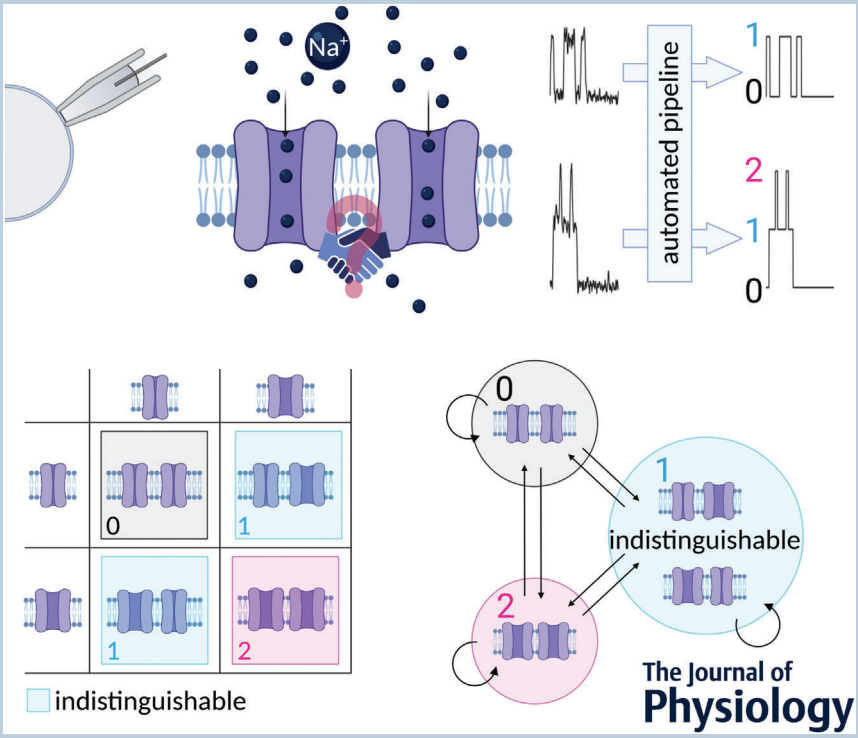

Abstract Cardiac voltage-gated sodium (Na^+) channels ($Na_v1.5$) are crucial for myocardial electrical excitation. Recent studies based on single-channel recordings have suggested that Na^+ channels interact functionally and exhibit coupled gating. However, the analysis of such recordings frequently relies on manual interventions, which can lead to bias. Here, we developed an automated pipeline to de-trend and idealize single-channel currents, and assessed possible functional

Zoja Selimi completed her studies in General Medicine at the University of Prishtina (Kosova) and is presently finishing her MD-PhD programme in the Integrative Cardiac Bioelectricity Group led by Professor Jan P. Kucera at the Department of Physiology of the University of Bern. Zoja enjoys patch-clamping, mathematics and writing computer programs, and she is eager to apply her knowledge in biology and medicine. Her research focuses on exploring the functional interactions between channels.

DOI: 10.1113/JP284861

interactions in cell-attached patch clamp experiments in HEK293 cells expressing human $Na_v1.5$ channels as well as in adult mouse and rabbit ventricular cardiomyocytes. Our pipeline involved de-trending individual sweeps by linear optimization using a library of predefined functions, followed by digital filtering and baseline offset. Subsequently, the processed sweeps were idealized based on the idea that the ensemble average of the idealized current identified by thresholds between current levels reconstructs at best the ensemble average current from the de-trended sweeps. This reconstruction was achieved by non-linear optimization. To ascertain functional interactions, we examined the distribution of the numbers of open channels at every time point during the activation protocol and compared it to the distribution expected for independent channels. We also examined whether the channels tended to synchronize their openings and closings. However, we did not uncover any solid evidence of such interactions in our recordings. Rather, our results indicate that wild-type $Na_v1.5$ channels are independent entities or exhibit only very weak functional interactions that are probably irrelevant under physiological conditions. Nevertheless, our unbiased analysis will be important for further studies examining whether auxiliary proteins potentiate functional Na^+ channel interactions.

(Received 11 April 2023; accepted after revision 23 June 2023; first published online 20 July 2023)
Corresponding author J. P. Kucera: Department of Physiology, University of Bern, Bühlplatz 5, CH-3012 Bern, Switzerland. Email: jan.kucera@unibe.ch

Abstract figure legend To examine whether cardiac voltage-gated Na^+ channels interact functionally, we conducted cell-attached patch-clamp recordings (top left) of two or more channels. To have a bias-free analysis, we developed an automated algorithm to idealize the recorded currents (top right). To quantify functional interactions, we used contingency tables (bottom left) under the assumption of identical and indistinguishable channels. In addition, we examined the transition rates between different compound states (bottom right). We did not find any evidence of coupled or cooperative gating.

Key points

- $Na_v1.5$ channels are critical for cardiac excitation. They are part of macromolecular interacting complexes, and it was previously suggested that two neighbouring channels may functionally interact and exhibit coupled gating.
- Manual interventions when processing single-channel recordings can lead to bias and inaccurate data interpretation.
- We developed an automated pipeline to de-trend and idealize single-channel currents and assessed possible functional interactions between $Na_v1.5$ channels in HEK293 cells and cardiomyocytes during activation protocols using the cell-attached patch clamp technique.
- In recordings consisting of up to 1000 sweeps from the same patch, our analysis did not reveal any evidence of functional interactions or coupled gating between wild-type $Na_v1.5$ channels.
- Our unbiased analysis may be useful in further studies examining how Na^+ channel interactions are affected by mutations and auxiliary proteins.

Introduction

Cardiac voltage-gated sodium channels ($Na_v1.5$), which carry the fast inward sodium current (I_{Na}), play a key role in the electrical excitation of the heart. I_{Na} underlies the rapid action potential upstroke and ensures action potential propagation across the working myocardium (Ahern et al., 2016; Hille, 2001; Kléber & Rudy, 2004). Mutations in *SCN5A*, the gene that encodes the pore-forming α-subunit of the $Na_v1.5$ channel, are tightly related to several arrhythmogenic disorders and structurally abnormal phenotypes such as Brugada syndrome, long-QT syndrome type 3, atrial fibrillation, sick sinus syndrome and dilated cardiomyopathy (Bezzina et al., 2003; Lieve & Wilde, 2015; McNair et al., 2004; Olson & Keating, 1996; Ruan et al., 2009; Veerman et al., 2015; Wilde & Amin, 2018). These conditions can precipitate sudden cardiac death.

However, similar pathological manifestations have been observed in patients without any *SCN5A* mutation, which led to the idea that the function of $Na_v1.5$ channels is tightly controlled by several regulatory proteins (Abriel et al., 2015; Rivaud et al., 2020). These interacting proteins play diverse roles, for example in membrane trafficking of the channels, in their anchoring to cytoskeletal proteins, in their post-translational modifications and in the regulation of their biophysical properties (Abriel et al., 2015; Dong et al., 2020). For instance, calmodulin regulates $Na_v1.5$ channel function, and mutations in either the binding site on $Na_v1.5$ or in calmodulin itself can reduce the peak of I_{Na} and destabilize its inactivation, leading to an increased persistent I_{Na} (Kang et al., 2021; Kim et al., 2004). Another interacting protein is 14-3-3η, and it has been suggested that this protein plays a role in Na^+ channel clustering and modifies the biophysical properties of I_{Na} by shifting its steady-state inactivation curve to more negative potentials (Allouis et al., 2006). In a recent study, Clatot et al. (2017) suggested that the α subunits of two Na^+ channels form dimers, and that two neighbouring channels can interact either directly or indirectly via the mediator protein 14-3-3η. Based on single-channel recordings in HEK293 cells expressing wild-type human Na^+ channels, the authors proposed that the biochemical interaction of these dimers may cause the sodium channels to also interact functionally by exhibiting cooperative gating, implying that the probability that the two channels are open simultaneously is increased (Clatot et al., 2017). In their experiments, the functional interaction was reduced by difopein, a protein that disrupts the interaction via 14-3-3η. However, the authors did not report any changes in the overall macroscopic behaviour of I_{Na} (Clatot et al., 2017). Thus, the cardiac Na^+ channel could be considered as a dimeric complex rather than a single functional unit.

The notion that Na^+ channels interact functionally represents a paradigm shift because it implies that the functional units of I_{Na} are channel dimers (or possibly multimers) rather than single channels. In a previous study, we developed a mathematical model of a pair of interacting channels compatible with the data of Clatot et al. (2017), and illustrated the implications of this interaction in causing the dominant negative effect of the BrS-causing p.L325R variant of the human $Na_v1.5$ channel (Hichri et al., 2020). However, the paradigm of functionally interacting Na^+ channels is still in its emergence and requires further investigation.

Therefore, to gain more detailed insights into the functional interactions between Na^+ channels and to understand their implications for physiology, biophysics, pathophysiology and modelling, we developed an automated pipeline to analyse cell-attached patch clamp recordings of Na^+ channel currents, and applied it to own recordings using HEK293 cells expressing human $Na_v1.5$ channels and in adult mouse and rabbit ventricular cardiomyocytes. Single-channel recordings and cell-attached recordings are indeed the most suitable approach to study the microscopic behaviour of ion channels. However, such recordings are corrupted by noise, baseline drift and capacitance artefacts. Very commonly, these disturbances are removed manually before further analysis. Moreover, the analysis frequently requires user-defined thresholds to identify channel openings and closings. This large number of manual interventions is highly prone to subjective bias and may lead to inaccurate data interpretation.

To minimize this bias, our analysis pipeline presented in this study has only a minimal set of parameters. It subtracts the capacitance artefacts and baseline drifts, idealizes the single-channel currents and counts the number of open channels at every time point during every recorded sweep. Then, we used different approaches to explore any significant interaction quantitatively. We generalized our previously published method (Hichri et al., 2020) to quantify the interaction between two or more identical and indistinguishable channels. Next, we applied a modification of the method proposed by Chung and Kennedy (1996) to investigate the tendency of channels to synchronize their openings and closings (coupled gating).

Overall, we did not find any evidence for a strong functional interaction in our recordings compared to what was reported by others (Clatot et al., 2017). Rather, our results indicate that wild-type $Na_v1.5$ channels are independent entities or exhibit only very weak functional interactions that are probably irrelevant under physiological conditions.

Methods

Ethical approval

The handling of animals was done in accordance with the ethical principles and guidelines of the Swiss Academy of Medical Sciences. The procurement of animals, husbandry and experiments were done according to the European Convention for the Protection of Vertebrate Animals used for Experimental and other Scientific Purposes. According to Swiss legislation, the protocols used here were approved and authorized by the Commission of Animal Experimentation of the Cantonal Veterinary Office of the Canton of Bern, Switzerland [authorizations BE 88/2022 (for mice) and BE 132/2020 (for rabbits)]. The experiments were conducted according to the animal welfare committee guidelines of the University of Bern, under the overarching framework of Swiss federal legislation and the guidelines of the Swiss Academy of Medical Sciences. The investigators understand the ethical principles under which the journal

operates and our work complies with the animal ethics checklist outlined in the editorial by Grundy (2015).

Cell culture and transfection

Modified human embryonic kidney (HEK) tsA201 cells (ECACC 96121229) were cultured in Dulbecco's modified Eagle medium (DMEM; Gibco, Basel, Switzerland) supplemented with 10% fetal bovine serum (FBS), 0.5% penicillin and streptomycin (10,000 U/mL) at 37°C in a 5% CO_2 incubator. The cells were transferred to 35 mm dishes and co-transfected, using LipoD293^{TM} (SL100668, SignaGen® Laboratories), with cDNAs coding for the pore-forming α-subunit of the h$Na_v1.5$ wild-type channel (varying quantities 0.25–1 μg), the β-auxiliary subunit h$Na_v1.5\beta1$ (0.5 μg) and the CD8 receptor (0.5 μg) as a reporter gene. The cells were transferred 18–24 h after transfection to new dishes, and 12–24 h thereafter they were used for patch-clamp experiments. For these experiments, anti-CD8 beads (Dynal®, Thermo Fisher Scientific, Oslo, Norway) were used and only cells decorated with anti-CD8 beads were investigated.

Isolation of mouse ventricular myocytes

Ventricular cardiomyocytes from wild-type adult C57BL/6J mice (own breeding at the Central Animal Facility of the Faculty of Medicine of the University of Bern) were isolated according to a modified procedure using established enzymatic methods (Boixel et al., 2006; Rougier et al., 2019). At least 7 days before the mice were killed, tunnel/cup handling procedures were performed to reduce the stress of the animals. The animals always had *ad libitum* access to food (standard diet) and water. The mice (n = 4 females, 23–28 weeks old, weighting 22–28 g) were deeply and terminally anaesthetized via an intraperitoneal injection of ketamine and xylazine (200 and 20 mg/kg body weight, respectively). To avoid blood coagulation inside the heart, which could interfere with the *ex vivo* procedures, heparin (5000 IU/mL, 4 mL/kg body weight) was also added to the anaesthesia mix. The depth of anaesthesia was assessed by the absence of the pedal withdrawal reflex. The animals were then killed by cervical dislocation before a thoracotomy was performed. Hearts were rapidly excised, cannulated and mounted on a Langendorff apparatus for retrograde perfusion (3 mL/min) at 37°C. The hearts were rinsed free of blood with a nominally Ca^{2+}-free solution containing (in mmol/L): NaCl, 135; KCl, 4; $MgCl_2$, 1.2; NaH_2PO_4, 1.2; HEPES, 10; glucose, 11; pH = 7.4 (adjusted with NaOH), and subsequently digested by a solution supplemented with 50 μM Ca^{2+} and collagenase type II (1 mg/mL, Worthington, Allschwil, Switzerland) for ∼15 min. Following digestion, the atria were removed, and the ventricles transferred to a nominally Ca^{2+}-free solution, where they were minced into small pieces. Single cardiac myocytes were liberated by gentle trituration of the digested ventricular tissue and filtered through a 100 μm nylon mesh.

Isolation of rabbit ventricular myocytes

Ventricular myocytes from adult wild-type New Zealand white rabbits were kindly provided by Katja Odening and her research group. The animals were bred at the Centre for Experimental Models and Transgenic Services, University Medical Centre, Freiburg, Germany, and housed at the Central Animal Facility of the Faculty of Medicine of the University of Bern. They were fed *ad libitum* (normal diet) and had constant access to water. The rabbits (n = 2 females, 6 months old, weight 3.8 kg) were anaesthetized by subcutaneous injection of ketamine and xylazine (12.5 and 3.75 mg/kg body weight, respectively) and anti-coagulated with an intravenous injection of heparin (1000 IU in 1 mL). The animals were then killed by using an intravenous injection of pentobarbital (150 mg/kg body weight). This was assessed by the cessation of breathing, dilated pupils and the absence of corneal reflex and pain reaction. The hearts were then excised and mounted on a Langendorff apparatus for enzymatic digestion with collagenase, as described in detail by Odening et al. (2019). These myocytes were obtained as leftover cells obtained in the context of separate studies by Katja Odening.

Electrophysiological recordings

Cell-attached patch clamp recordings were acquired using the integrating head stage mode for quiet single-channel recordings (β configuration was set to Patch) of an Axopatch 200B amplifier (Molecular Devices Corp., Sunnyvale, CA, USA). The gain was set to α = 10. Experiments were controlled using pClamp10 software (Molecular Devices). Currents were filtered with a 5 kHz four-pole Bessel filter and digitized at a sampling rate of 100 kHz. The bath solution contained (in mmol/L): KCl, 140; NaCl, 5; $MgCl_2$, 3; EGTA, 2; glucose, 6; HEPES, 10 at a pH = 7.4 adjusted with CsOH. The high potassium concentration in the bath ensured that resting membrane potential was brought near zero and thus facilitated control of the transmembrane voltage of the part of the cell membrane under the pipette. The pipette solution contained (in mmol/L): NaCl, 140; TEA-Cl, 30; $CaCl_2$,0.5; HEPES, 10 (nifedipine, 0.002, was used to inhibit $Ca_v1.2$ calcium channels when recording Na^+ currents in cardiomyocytes) at pH = 7.4 adjusted with CsOH. Patch pipettes with a resistance of 5–12 MΩ were pulled from quartz capillaries (QF150-75-10; Sutter Instruments,

Hofheim, Germany) using a P2000 laser puller (Sutter Instruments). The pipettes were coated with Sylgard® (Sigma-Aldrich, St. Louis, MO, USA) to decrease their wall capacitance. Pipette capacitance was compensated for to minimize the capacitive transient as far as possible. Cell-attached recordings were conducted upon a 50 ms depolarizing step to −60, −40 or −20 mV from a holding potential of −120 mV, and the recordings were repeated every 1 s. Sweeps were continuously acquired until their number reached 1000 or until the seal was lost. For the determination of single-channel conductance, 50 sweeps were acquired. The recordings were obtained at room temperature (22–23°C). Recordings were pursued only if seal resistance was >10 GΩ. Recordings from the isolated myocytes were conducted on the lateral membrane.

Data analysis

Cell-attached recordings were analysed using custom MATLAB programs (MathWorks, Natick, MA, USA). The programs build up an automated pipeline that comprises multiple steps (Fig. 1). Of note, in the cell-attached mode, inward Na^+ currents have a positive sign and are acquired as such. Thus, in this work, Na^+ currents were considered to be positive and their sign was not inverted in the analysis and graphical representations.

Overview of the analysis

As illustrated in Fig. 1, raw single-channel recordings are always corrupted by capacitance artefacts, baseline

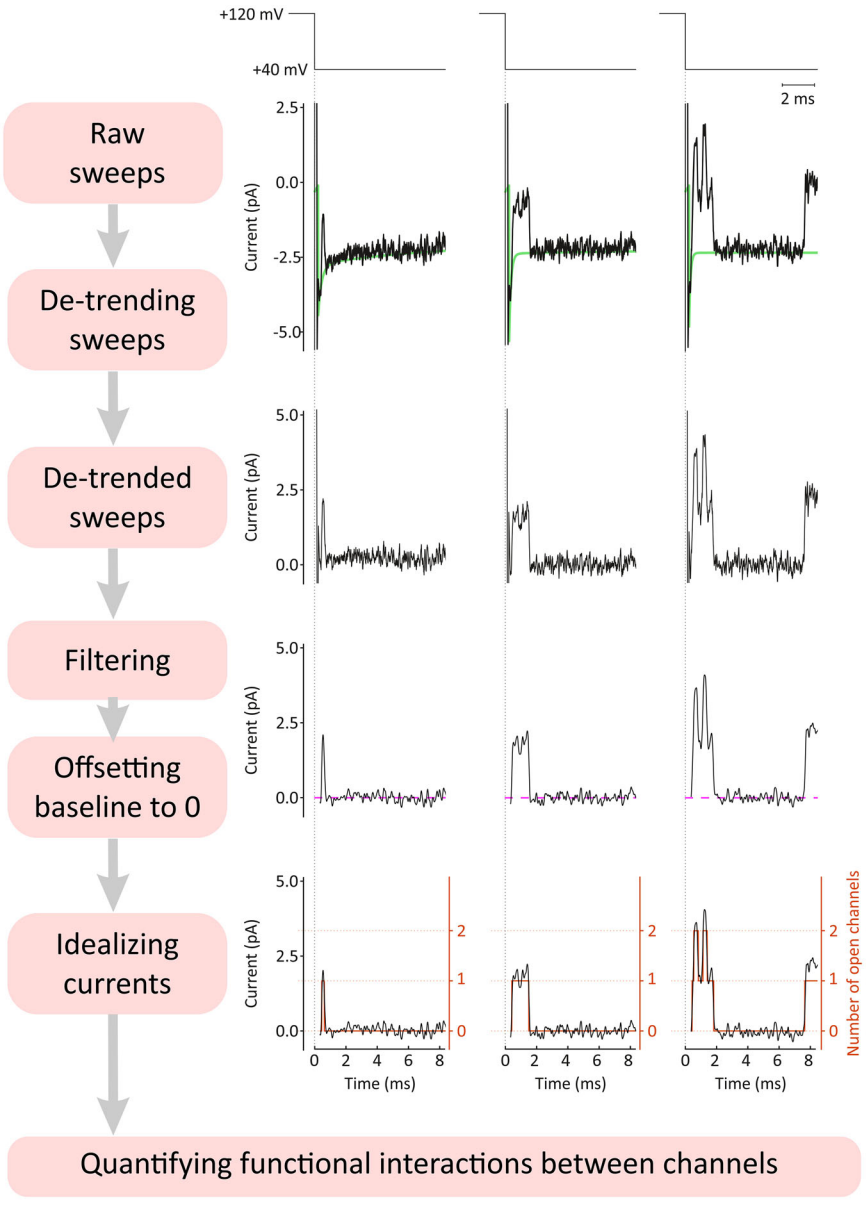

Figure 1. Analysis pipeline
The pipeline is illustrated by the flowchart on the left. *First row*: example sweeps obtained from a patch in an HEK cell upon application of a voltage step from +120 to +40 mV (corresponding, in the cell-attached mode, to a membrane depolarization from −120 to −40 mV). The voltage step was applied at time 0. The thick green curves represent the trends identified by the de-trending algorithm. *Second row*: sweeps after subtraction of the trends. *Third row*: de-trended sweeps after digital filtering (in this example: low-pass with 3.7 kHz cut-off frequency) and offsetting the baseline (absence of any open channel) to 0. *Fourth row*: idealization of the single-channel currents (orange, number of open channels *vs.* time).

drifts and high-frequency noise. Therefore, in a first step, capacitive artefacts and baseline drifts were identified and subtracted in every recorded sweep using a library of exponential and linear functions by applying an algorithm developed by (Abrams et al., 2020; Kang et al., 2021). In a second step, the resulting de-trended sweeps were optionally low-pass filtered. In a third step, the baseline of the de-trended and filtered sweeps (i.e. the current in the absence of any open channels) was offset to 0.

Idealizing the currents represented the fourth step of the processing pipeline. Here, we developed a new approach based on the idea that the ensemble average of the idealized currents should deviate as little as possible from the ensemble average current of the processed sweeps recorded from a given patch. In detail, the idealized current levels were determined iteratively (assuming that all channels produce the same current) using a non-linear procedure minimizing the mean square residual. This procedure was repeated under the assumption of a given number of channels (increasing from one to five), and the residual converged when the maximal number of simultaneous openings was identified (Fig. 2).

To explore functional interactions between channels, we counted, for every time point during the voltage clamp protocol, the number of simultaneously open channels and calculated the distribution of the fractions of sweeps with k open channels (f_k), with k ranging from 0 to the number of channels in the patch. Under the assumption of identical and indistinguishable channels, the probability that a channel is open (p_{open}) was calculated from the distribution f_k. Then, from p_{open}, the binomial distribution $\overline{f_k}$ that would be expected for channels that do not interact functionally (i.e. independent channels) was computed. Next, we compared statistically the observed and expected distributions f_k and $\overline{f_k}$ (multiplied by the number of sweeps) using the χ^2 test. For the case of two channels, this approach corresponds to the analysis of a contingency table, as illustrated in the bottom left panel of the Abstract Figure. To quantify the

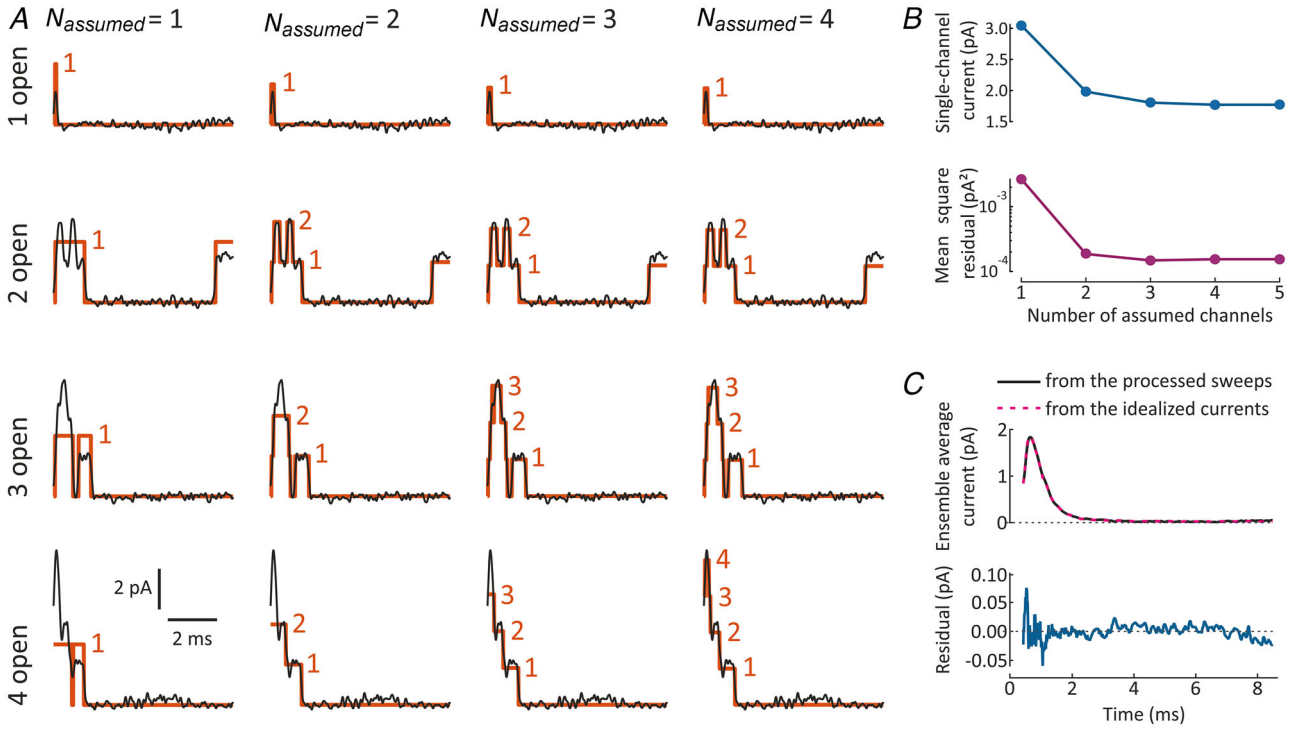

Figure 2. Idealization of single-channel currents
A, de-trended and baseline offset sweeps (black) recorded from an HEK cell membrane patch depolarized to −40 mV that exhibited up to four simultaneously open channels. The same sweeps are replicated in every column, whereby only one channel was open in the first row, two were simultaneously open in the second, three in the third and four in the fourth (labels). The orange trace represents the idealized currents together with the number of simultaneously open channels, under the assumption of one to four channels present in the patch (columns, labels). *B*, mean square residual (top) and single-channel current (bottom) output by the idealization algorithm under the assumption of one to five channels in the patch. *C*, ensemble average current (of 516 sweeps, top) computed from the processed sweeps and from the idealized currents, as well as the residual (bottom) under the assumption of $N_{assumed} = 4$ channels. The voltage step was applied at time $t = 0$. Note that the analysis was started at $t = 0.38$ ms because the very large capacitive artefact (orders of magnitude larger than the single-channel currents, see Fig. 1) could not be fully and reliably de-trended before that time.

interaction, we also computed the difference of the Shannon entropies (Shannon, 1948) of the distributions f_k and $\overline{f_k}$; this entropy difference is expected to be 0 for independent channels and negative for functionally interacting channels. To quantify the strength of the interaction between channels, we calculated the relative differences ε_k between f_k and $\overline{f_k}$ in a small time window centred around the peak of p_{open}. In the presence of cooperative gating, we always expect ε_1 to be negative.

In addition, we examined if the channels have a tendency to synchronize their openings and closings by inspecting the transition rates over a predefined time interval between configurations with given numbers of open channels (arrows in the bottom right panel of the Abstract Figure). These rates were compared to those that would be expected for non-interacting channels using an approach inspired by the work of Chung and Kennedy (1996). For two channels exhibiting coupled openings, the observed transition rate from zero ot two open channels is expected to be larger than that without interaction. Conversely, for two channels exhibiting coupled closings, the observed transition rate from two to zero open channels is expected to be larger than that without interaction.

The de-trending, filtering and idealization pipeline as well as the functions used to assess channel interactions were incorporated into user-friendly MATLAB graphical interfaces that are available to the scientific community on the repository Zenodo (https://doi.org/10.5281/zenodo.7817601). Technical and mathematical details of our analysis are provided in the remainder of the Methods section.

Details of the analysis

Step 1: The first step involves subtracting the capacitance artefact and the baseline drift from each individual sweep by using a library of functions, as described by Kang and colleagues (Abrams et al., 2020; Kang et al., 2021). This library contains predefined functions to remove the capacitive artefact as well as linear drifts and constant offsets. In our application, the library contains 25 decaying exponential functions with time constants ranging from 0.05 to 7.40 ms in a geometric progression as well as one linear and one constant function. In this de-trending process, the following cost function is minimized:

$$\min_{E,s|s\rangle 0}\left(\frac{1}{2}\left\|I_{measured}-D\cdot E-s\right\|_2^2+\lambda\left\|s\right\|_1\right)$$

where

$$E_{fit}=D\cdot E$$

and

$$I_{DE}=I_{measured}\ -E_{fit}$$

$I_{measured}$ is the raw sweep from a recording (in the form of a column vector of $N_{samples}$ elements, $N_{samples}$ being the number of time samples), while D is an $N_{samples}\times n_E$ matrix containing, in its columns, the $n_E = 27$ library functions, and E is a vector of corresponding n_E coefficients. The vector s (with $N_{samples}$) represents an estimation of positive outliers (samples >0) corresponding to the actual current through one or several Na^+ channels. The parameter λ is a regularization penalty parameter for the optimization problem, which should be set at a value not exceeding the root mean square (RMS) noise level. The vertical line brackets $\|\cdot\|_2$ and $\|\cdot\|_1$ represent the L^2 and L^1 norms, respectively. E_{fit} is the fitted capacitive transient and linear drift, and I_{DE} is the de-trended current that is left after subtracting this capacitive and baseline drift fit from the raw current. The cost function was minimized using an iterative steepest gradient descent algorithm [MATLAB code developed by Kang and colleagues (Abrams et al., 2020; Kang et al., 2021) and kindly provided by Manu Ben-Johny, Columbia University]. In our application, we observed that setting λ to 0.01 pA (5% of a typical RMS noise level of 0.20 pA) and 500–800 iterations always led to a good performance. In the original algorithm, the coefficients in the vector E are constrained to be zero or positive (Abrams et al., 2020; Kang et al., 2021), but in some circumstances, a better fit was obtained without constraint on the coefficients in E.

Step 2: In a second step, if necessary, the de-trended current was digitally filtered using a 3.7 kHz low-pass filter. This filtering was conducted using convolution with a Gaussian kernel. In many cases, filtering was not necessary due to the good quality of the raw signal.

Step 3: The algorithm of Kang and colleagues (Abrams et al., 2020; Kang et al., 2021) performs well to de-trend the signal, up to a constant offset term which depends on the parameter λ. Therefore, in this third step, the baseline was offset to 0 according to the following algorithm based on the assumptions that (i) for a given patch, there is a certain fraction of blank sweeps (in our experiments, this fraction was usually >10%), (ii) in every sweep, all channels are closed for a certain period of time (which is usually the case for a small number of Na^+ channels) and (iii) the single-channel current is larger than the peak-to-peak noise (which was the case in our recordings). The sweeps were ranked by peak-to-peak amplitudes, and the fraction f_{blank} of sweeps with the lowest peak-to-peak amplitudes was extracted and their samples were pooled together; this pool of samples served to estimate the peak-to-peak noise level I_{pp} of the recordings. The value of the parameter f_{blank} was set by default to 0.1. Then, the sweeps having a peak-to-peak amplitude lower than θI_{pp} (where θ is a parameter used as a multiplicative threshold) were categorized as blank, and these sweeps were used to estimate the mean residual current μ. A default value of

2 was used for the parameter θ. For every sweep, the subset of samples in the interval $[\mu - I_{pp}/2,\ \mu + I_{pp}/2]$ was extracted, a Gaussian function was fitted to the histogram of this subset of samples and the fitted peak of this Gaussian was subtracted from the sweep.

Step 4: The next step is the idealization of the de-trended and baseline offset current sweeps, $I_{sweep,i}$, with the index i going from 1 to the number of utilizable sweeps, N_{sweeps}. The novel idea behind this step is that the ensemble average of the idealized sweeps ($E_{idealized}$), identified by thresholds between current levels, must reconstruct at best the ensemble average current of the de-trended sweeps (E_{sweeps}). $E_{idealized}$ is defined as

$$E_{idealized}(t) = \frac{1}{N_{sweeps}} \sum_{i=1}^{N_{sweeps}} I_{idealzed,i}(t)$$

where $I_{idealzed,i}$ is the ith idealized sweep, and the ensemble average current of the de-trended sweeps is computed as

$$E_{sweeps}(t) = \frac{1}{N_{sweeps}} \sum_{i=1}^{N_{sweeps}} I_{sweep,i}(t)$$

The sweeps are idealized by identifying thresholds between current levels corresponding to zero, one, two, etc., simultaneously open channels, up to the maximal number (N_{max}) of simultaneously open channels in a given set of sweeps (corresponding to a single membrane patch). Of note, this maximal number is not necessarily equal to the actual number of channels present in the patch, but it is in no case greater than it. Assuming that the channels have an identical unitary current i_u, the current levels are equally spaced from i_0 to $i_0 + N_{max} i_u$, where i_0 is the zero-current level (in the absence of any open channel). We then set the thresholds at the mid-points between these levels and idealized the sweeps by rounding every individual sample to the nearest current level.

The aim of the idealization algorithm is to find the values of i_0 and i_u that minimize a cost function defined by the difference between E_{sweeps} and $E_{idealized}$. As a cost function, we used the L^2 norm of this difference divided by the number of time samples ($N_{samples}$), that is the mean square residual (R^2) defined as

$$R^2 = \frac{1}{N_{samples}} \sum_{j=1}^{N_{samples}} \left(E_{sweeps}(t_j) - E_{idealized}(t_j)\right)^2$$

where t_j is the time of the jth sample.

Due to the thresholding procedure, R^2 (a function of i_0 and i_u) is piecewise constant and thus discontinuous in the i_0–i_u parameter space. Hence, any minimization algorithm can easily miss the true minimum of R^2. Therefore, the computation of R^2 was regularized by introducing a regularization parameter ρ to smooth the transition over the thresholds, as follows.

The thresholds θ_k between the kth and the k+1th current levels were defined as

$$\theta_k = i_0 + \left(k + \frac{1}{2}\right) i_u$$

Then, for every sample s from $I_{sweep,i}(t)$, a set of auxiliary variables p_k (with k ranging from 0 to N_{max}) was defined as

$$p_0 = 1 - \frac{1}{1 + e^{(\theta_1 - s)/\rho}}$$

$$p_{k,0<k<N_{max}} = \frac{1}{1 + e^{(\theta_k - s)/\rho}} - \frac{1}{1 + e^{(\theta_{k+1} - s)/\rho}}$$

$$p_{N_{max}} = \frac{1}{1 + e^{(\theta_{N_{max}} - s)/\rho}}$$

The values of p_k can be intuitively understood as the 'probability' that sample s corresponds to the current carried by k open channels. The idealized sample $s_{idealized}$ was then computed as

$$s_{idealized} = \sum_{k=0}^{N_{max}} p_k (i_0 + k i_u)$$

These idealized samples served to construct the idealized sweeps, their ensemble average $E_{idealized}$ and to compute R^2, now a continuous function of i_0 and i_u. Of note, in the limit as ρ approaches 0, the procedure outlined above corresponds to rounding the samples to the nearest current level.

Starting with $\rho = 0.04$ pA (∼20% of the typical RMS noise level of 0.20 pA), the minimum of R^2 was identified using the Nelder–Mead downhill simplex method (function 'fminsearch' in MATLAB) (Nelder & Mead, 1965). As initial guesses, a value of 0 was used for i_0 and the initial guess of i_u was estimated from a priori knowledge of the single-channel current (typically 1.5–2.5 pA) expected at a given step potential or directly from a rapid visual inspection of the sweeps. The minimization algorithm was then re-run a further seven times after halving ρ every time, with initial guesses provided by the values of i_0 and i_u minimizing R^2 in the previous run. At the end, the algorithm was run with $\rho = 0$. This iterative procedure resulted in robust convergence insensitive to the initial guess of i_0 and i_u.

An initial execution of the algorithm was carried out with $N_{max} = 1$, providing optimized values of i_0, i_u and R^2. The algorithm was then repeated with increasing values of N_{max}. Incrementing N_{max} led to a convergence of R^2 as well as of i_0 and i_u. Increasing N_{max} further then did not improve the minimization of R^2. Therefore, the value of N_{max} for which R^2 reached its minimum was considered as the correct estimate of the maximal number

of simultaneously open channels in an experiment with a given patch.

At the end of this idealization step, the algorithm then outputs the number of open channels at every sample of every sweep.

Quantification of the interaction between channels

To explore if there is any significant interaction between channels under non-stationary conditions, we generalized our previously published approach (Hichri et al., 2020). This generalization allows us to quantify the interaction between two or more channels under the assumptions that all the channels are identical and indistinguishable and that the action of one channel on another is reciprocal. After obtaining the idealized traces, our program counts the number of sweeps containing $0,\ 1,\ 2, \ldots,\ N_{max}$ open channels as a function of time. These counts correspond to current levels $L_k(t)$, with $k \in \{0,\ 1,\ 2, \cdots, N_{\max}\}$ and $\sum_{k=0}^{N_{max}} L_k\ (t) = N_{sweeps}$. The respective fractions were calculated as $f_k(t) = \frac{L_k(t)}{N_{sweeps}}$, and hence $f_k(t)$ denotes the fraction of sweeps having k channels open at time t. In the limit of a large number of sweeps, these fractions approach the true probabilities of observing a given number of open channels at a given time during the voltage clamp protocol. The set $\{f_0(t),\ f_1(t),\ f_2(t),\ \ldots,\ f_{N_{max}}(t)\}$ forms a sample from a discrete $N_{max} + 1$-element distribution. From the distribution of these counts, the binomial distribution expected for independent non-interacting channels was calculated as follows. First, an assumption must be made regarding the number of channels actually present in the patch ($N_{assumed}$), a number that is necessarily greater than or equal to N_{max}, the maximal number of simultaneously open channels observed in a given patch. From the assumption that the channels are identical, the probability (fraction of cases) that any given channel is open (p_{open}) or respectively shut (i.e. closed or inactivated) is computed as

$$f_{N_{assumed},shut}\ (t) = \sum_{k=0}^{N_{assumed}-1} \left(\frac{(N_{assumed} - k)}{N_{assumed}} \cdot f_k\ (t) \right)$$

$$p_{open} = f_{N_{assumed},open}\ (t) = \sum_{k=1}^{N_{assumed}} \left(\frac{k}{N_{assumed}} \cdot f_k\ (t) \right)$$

$$= 1 - f_{N_{assumed},shut}\ (t)$$

where $f_{N_{assumed},shut}$ and $f_{N_{assumed},open}$ are respectively the fractions of channels being shut and open. These fractions are calculated from the fractions yielded by the observed counts. From these, using the binomial distribution formula, we compute the fractions of sweeps $\overline{f_k}$ and the number of sweeps $\overline{L_k}$ that would be expected to yield k open channels at time t in the absence of any interaction (the overbar indicates expected values without interaction) as

$$\overline{f_k}\ (t) = \binom{N_{assumed}}{k} \cdot f_{N_{assumed},shut}^{N_{assumed}-k}\ (t) \cdot f_{N_{assumed},open}^{k}\ (t)$$

$$\overline{L_k}\ \ (t) = N_{sweeps}\ \cdot \overline{f_k}\ (t)$$

Thus, the set $\{\overline{f_0}(t),\ \overline{f_1}(t),\ \overline{f_2}(t),\ \ldots,\ \overline{f_n}(t)\}$ forms a sample from a binomial distribution.

The significance of the difference between the observed distribution of counts $\{L_0(t),\ L_1(t),\ L_2(t),\ \ldots,\ L_{N_{assumed}}(t)\}$ and the expected distribution $\{\overline{L_0}(t),\ \overline{L_1}(t),\ \overline{L_2}(t),\ \ldots,\ \overline{L_{N_{assumed}}}(t)\}$ was ascertained using the χ^2 test. This χ^2 test typically yielded p-values that fluctuated between 0 and 1, with values sometimes near 0. However, one must here keep in mind that one or only a few p-values lower than a predefined threshold (e.g. 0.05) does not imply significance, because repeated testing was conducted at every time point. Moreover, it must be noted that $p_{open}(t)$ as well as $f_k(t)$ and $\overline{f_k}(t)$ are auto-correlated signals because their temporal variations are small and progressive rather than large and abrupt from sample to sample. For this reason, classical correction methods (such as Bonferroni correction) cannot be applied. In the presence of a truly significant interaction, however, one can expect that the p-value will remain lower than a predefined threshold for a substantial period of time. Thus, we considered the interaction to be significant only when p remained below 0.05 for at least 0.5 ms (50 samples).

The difference between the distributions $\{f_0(t),\ f_1(t),\ f_2(t),\ \ldots,\ f_{N_{assumed}}(t)\}$ and $\{\overline{f_0}(t),\ \overline{f_1}(t),\ \overline{f_2}(t),\ \ldots,\ \overline{f_{N_{assumed}}}(t)\}$ was also quantified using the difference between the Shannon entropies (Shannon, 1948) of these distributions as follows:

$$S\ (t) = -\sum_{k=0}^{N_{assumed}} f_k\ (t) \cdot \log \frac{f_k\ (t)}{\binom{N_{assumed}}{k}}$$

$$\bar{S}\ (t) = -\sum_{k=0}^{N_{assumed}} \overline{f_k}\ (t) \cdot \log \frac{\overline{f_k}\ (t)}{\binom{N_{assumed}}{k}}$$

$$\Delta S\ (t) = S\ (t) - \bar{S}\ (t)$$

where $S(t)$ and $\bar{S}(t)$ represent Shannon's entropy of the observed and expected distributions, respectively. The entropy difference $\Delta S(t)$ quantifies the interaction at any time point based on the information that is lost by assuming independent (i.e. non-interacting) channels. If the channels do not exhibit any interaction, $\Delta S(t)$ is expected to be 0. Otherwise, $\Delta S(t)$ is expected to be negative.

The binomial coefficients in the denominators take into account that there are $\binom{N_{assumed}}{k}$ possible arrangements of k open channels among a total of $N_{assumed}$. Because the channels are identical, each arrangement then has the same probability. The entropy is maximized by the binomial distribution.

To quantify the strength of the interaction between channels, we calculated (for $k \in \{1, 2, \cdots N_{assumed}\}$) the relative difference between f_k and $\overline{f_k}$ in a small time window (0.4 ms, unless specified otherwise) centred around the peak open probability (the peak of $f_{N_{assumed},open}$). Specifically, we calculated the means μ_k and $\overline{\mu_k}$ of f_k and $\overline{f_k}$, respectively, within this time window, and quantified the effect as the relative change of μ_k with respect to and $\overline{\mu_k}$ as

$$\varepsilon_k = \frac{\mu_k - \overline{\mu_k}}{\overline{\mu_k}}$$

The presence of an interaction will lead to $\varepsilon_k \neq 0$ for some of the k values. For the case of two channels with cooperative gating, we expect ε_1 to be negative and ε_2 to be positive. Even with more than two channels, we always expect ε_1 to be negative.

The approach presented above detects deviations of the distribution of the f_k values from the binomial distribution expected in the absence of interactions. However, this approach does not provide any direct information regarding the tendency of channels to synchronize their openings or closings (coupled gating). To gain such information, we implemented an approach based on the work of Chung and Kennedy (1996).

We consider a collection of N identical channels that can be either shut or open at arbitrary predefined times t_1 and t_2 during the voltage clamp protocol, with $t_1 < t_2$. By counting the number of sweeps in which there are i channels open at time t_1 and j channels open at time t_2 and by dividing this number by the number of sweeps in which there are i channels open at time t_1, we can obtain an estimate of the transition probability (during that time interval) from a configuration with i open channels to one with j open channels. These probabilities can be arranged as an $N+1$ by $N+1$ matrix as

$$A_{t_1\to t_2} = \begin{pmatrix} r_{0\to 0} & r_{1\to 0} & \cdots & r_{N\to 0} \\ r_{0\to 1} & r_{1\to 1} & & r_{N\to 1} \\ \vdots & & \ddots & \vdots \\ r_{0\to N} & r_{1\to N} & \cdots & r_{N\to N} \end{pmatrix}, \text{ with}$$

$$\sum_{j=0}^{N} r_{i\to j} = 1 \text{ for all } i,$$

where $r_{i\to j}$ is the conditional probability (or the fraction of observations) of having j channels open at time t_2 when there were i channels open at time t_1. For the particular case with only one channel ($N = 1$), we have

$$V_{t_1\to t_2} = \begin{pmatrix} r_{0\to 0} & r_{1\to 0} \\ r_{0\to 1} & r_{1\to 1} \end{pmatrix} = \begin{pmatrix} 1-\alpha & \beta \\ \alpha & 1-\beta \end{pmatrix},$$

where α and β can be understood as opening and closing probabilities over the interval from t_1 to t_2.

Note that, in general, for channels having more than one open or more than one shut configuration (as is the case for Na^+ channels), the matrices $A_{t_1\to t_2}$ and $V_{t_1\to t_2}$ as well as the values of α and β depend on both t_1 and t_2 and not only on the time interval $\Delta t = t_2 - t_1$. The reason for this is the non-stationary behaviour of our collection of channels, which, in their ensemble average, exhibit a transient behaviour (activation and inactivation). Chung and Kennedy analysed only stationary recordings, which made it possible to pool together all transition counts for all possible intervals of one sampling period; however, in our case, such pooling cannot be conducted because of non-stationarity.

Chung and Kennedy (1996) described in detail how to derive A from V (i.e. from α and β) for any N using Kronecker products and further matrix operations under the assumption that the channels are independent. Importantly, this derivation does not require stationarity. For example, for $N = 2$,

$$\bar{A}_{t_1\to t_2} = \begin{pmatrix} (1-\alpha)^2 & \beta(1-\alpha) & \beta^2 \\ 2\alpha(1-\alpha) & (1-\alpha)(1-\beta)+\alpha\beta & 2\beta(1-\beta) \\ \alpha^2 & \alpha(1-\beta) & (1-\beta)^2 \end{pmatrix},$$

where the overbar indicates the assumption of independence and distinguishes it from the matrix $A_{t_1\to t_2}$ estimated from experimental data. The key step is then to find the values of α and β that yield $\bar{A}_{t_1\to t_2}$ that fits the observed $A_{t_1\to t_2}$ at best. As a measure of the quality of the fit, we used $\|A_{t_1\to t_2} - \bar{A}_{t_1\to t_2}\|_2$, the Frobenius norm of the difference between the two matrices and minimized it using the algorithm of Nelder and Mead (1965).

By examining the entries of $A_{t_1\to t_2}$ and $\bar{A}_{t_1\to t_2}$, information can then be obtained regarding whether transitions between configurations with given numbers of open channels are favoured or not by a possible interaction. For example, for $N = 2$, $r_{0\to 2} > \bar{r}_{0\to 2}$ suggests coupled openings while $r_{2\to 0} > \bar{r}_{2\to 0}$ suggests coupled closings during the interval from t_1 to t_2. In our concrete application, we selected a predefined interval Δt of 0.05 ms, computed $A_{t_1\to t_2}$ and $\bar{A}_{t_1\to t_2}$ with t_1 sliding along the voltage clamp protocol and $t_2 = t_1 + \Delta t$. Then, we inspected whether plots of corresponding entries of $A_{t_1\to t_2}$ and $\bar{A}_{t_1\to t_2}$ *vs.* t_1 overlapped or not.

Results

Pipeline for the analysis of single-channel recordings

Figure 1 illustrates our automated analysis pipeline. The first three rows in Fig. 1 show example current sweeps recorded in the cell-attached mode from an HEK cell upon repetition of a depolarizing voltage step, the trends identified by the de-trending algorithm, the sweeps after subtracting these trends, and the corresponding sweeps after digital filtering and automated baseline offset. The bottom row in Fig. 1 shows the de-trended sweeps together with their idealization. In this example, maximally one channel was open in the first two sweeps, whereas up to two channels were open together in the third sweep.

The idealization algorithm is illustrated in Fig. 2. Figure 2*A* shows sweeps from an HEK cell patch that exhibited up to four open channels simultaneously. In the first column of Fig. 2*A*, the algorithm was run under the assumption of $N_{assumed} = 1$ channel in the patch. Under this assumption, the single-channel current was clearly overestimated (orange traces) and the algorithm failed to detect multiple opening levels. With $N_{assumed} = 2$, the algorithm performed better, but failed to idealize the current levels with three or four simultaneous openings. Performance was further improved with $N_{assumed} = 3$ (third column), whereby the simultaneous opening of four channels was still poorly detected. In contrast, optimal performance was achieved with $N_{assumed} = 4$ (fourth column). Figure 2*B* shows the convergence of both the identified single-channel current and the mean squared difference (residual) between the ensemble average current computed directly from all the sweeps of this experiment (516 successfully recorded sweeps before the seal was lost) and the ensemble average of the idealized currents. The performance of the algorithm was not improved by increasing $N_{assumed}$ beyond 4. Thus, there were at most four channels open simultaneously in this experiment. Figure 2*B* illustrates the precise reconstruction of the ensemble average current by our algorithm with a low residual, for $N_{assumed} = 4$.

Scarce evidence of cooperative channel interactions in the HEK cell expression system as well as in isolated cardiomyocytes

Idealized currents output by the automated algorithm were then used to ascertain whether cooperative functional channel interactions were present in our cell-attached patch clamp recordings. Specifically, we ascertained whether the distribution of the number of open channels *vs.* time deviates from the binomial distribution that would be predicted in the absence of interactions. Figure 3 illustrates an experiment with an HEK cell expressing human $Na_v1.5$ channels. In this experiment, 160 successive sweeps were recorded

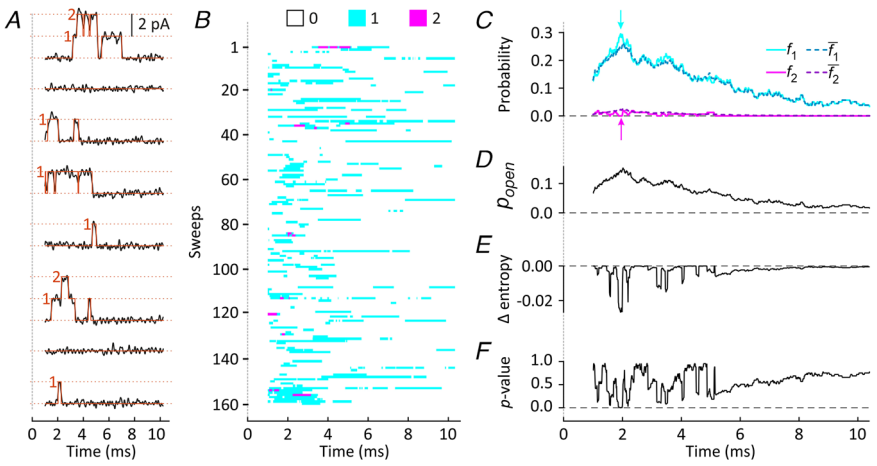

Figure 3. Analysis of $hNa_v1.5$ channel interactions in an HEK cell patch based on the expected binomial distribution
A, example sweeps (black, de-trended and filtered) recorded from an HEK cell patch containing two human $Na_v1.5$ channels depolarized (at time 0) to −60 mV, together with the idealized current (orange) permitting quantification of the number of open channels. *B*, colour map representation of the idealized 160 consecutive sweeps successfully recorded with this protocol. *C*, observed fractions of sweeps (continuous traces) with one open channel (f_1, cyan) or two open channels (f_2, magenta) and expected fractions (binomial distribution) without interaction ($\overline{f_1}$, sea blue, and $\overline{f_2}$, purple dotted traces). Arrows indicate the larger f_1 (cyan) relative to $\overline{f_1}$ (sea blue) and the smaller f_2 (magenta) relative to $\overline{f_2}$ (purple). *D*, single-channel open probability. *E*, entropy difference between the observed and expected distributions. *F*, *p*-value of the χ^2 test comparing the expected and observed distributions. The same analysis was conducted at every sample time.

upon application of the voltage protocol before the seal became unstable and was eventually lost. Figure 3*A* shows example sweeps and Fig. 3*B* shows the idealization of the 160 sweeps in the form of a colour map. This map shows that there was no manifest rundown of the preparation. While most channel activity occurred at the L_1 level (cyan), there were occasional simultaneous openings of the two channels (L_2 level, magenta). Figure 3*C* shows the observed fractions f_1 and f_2 of sweeps exhibiting, at every individual time point, one or two open channels, together the fractions $\overline{f_1}$ and $\overline{f_2}$ that would be expected without channel–channel interactions (independent channels). Figure 3*D* shows the corresponding single-channel open probability p_{open} (i.e. the fraction of open channels, assuming that the channels are identical), which peaked at 0.16 at time $t = 2$ ms. There was no large difference between observed (f_1 and f_2) and expected ($\overline{f_1}$ and $\overline{f_2}$) fractions. In a window of 0.4 ms centred about the peak open probability, f_1 was only slightly larger than $\overline{f_1}$ while f_2 was less than $\overline{f_2}$ (coloured arrows in Fig. 3*C*). Quantitatively, ε_1 amounted to 0.11 (positive) while ε_2 was −0.72 (negative), which in fact suggests against cooperative gating.

The difference in Shannon's entropy between the observed and expected distributions fluctuated between 0 and −0.025 and remained altogether small (Fig. 3*E*). The χ^2 test comparing these distributions yielded *p*-values that fluctuated erratically between 0 and 1 (Fig. 3*F*), and the duration of the longest segment during which *p* remained <0.05 was 0.13 ms, near the peak of p_{open}. In summary, the results of this experiment do not reveal any strong or significant interaction between the channels.

Figure 4 depicts an experiment and the corresponding analysis for an isolated murine ventricular myocyte, in a manner similar to that in Fig. 3. The membrane patch, containing two Na^+ channels, was stepped to a membrane potential of −40 mV. Figure 4*A* shows examples among the 100 successfully recorded sweeps. The full set of 100 idealized sweeps is shown as a colour map in Fig. 4*B*. As shown in Fig. 4*C*, the observed fractions of sweeps with respectively one and two open channels did not manifestly differ from the fractions expected based on the binomial distribution, as can be appreciated from the overlap of corresponding solid and dotted traces. Peak open probability reached its maximum of 0.43 at near $t = 0.5$ ms (Fig. 4*D*). Quantitatively, ε_1 was −0.01 while ε_2 was 0.02. Similarly to the experiment shown in Fig. 3, the entropy difference fluctuated between 0 and −0.025 (Fig. 4*E*). The *p*-value of the χ^2 test fluctuated between 0 and 1 (Fig. 4*F*) and the duration of the longest segment with $p < 0.05$ was 0.06 ms, in a narrow interval occurring at a time clearly falling into the macroscopic inactivation process (reflected by the time course of single-channel open probability p_{open}), but comprising only a small segment of inactivation. Thus, there was no significant cooperation (or antagonism) between the channels.

An experiment with an isolated rabbit ventricular myocyte is shown in Fig. 5, in which currents from two Na^+ channels (Fig. 5*A*) were recorded from the patch and idealized (Fig. 5*B*). As shown in Fig. 5*C*, contrary to the anticipation of finding $f_1 < \overline{f_1}$ and $f_2 > \overline{f_2}$ based on the hypothesis of cooperative gating, the observed f_1 was larger than the expected $\overline{f_1}$ and f_2 was smaller than the expected $\overline{f_2}$ in the period preceding the peak of open probability (corresponding to macroscopic activation shown in Fig. 5*D*, see coloured arrows in Fig. 5*C*), with $\varepsilon_1 = 0.05$ and $\varepsilon_2 = -0.01$. This behaviour was similar to that shown in Fig. 3. The entropy difference between

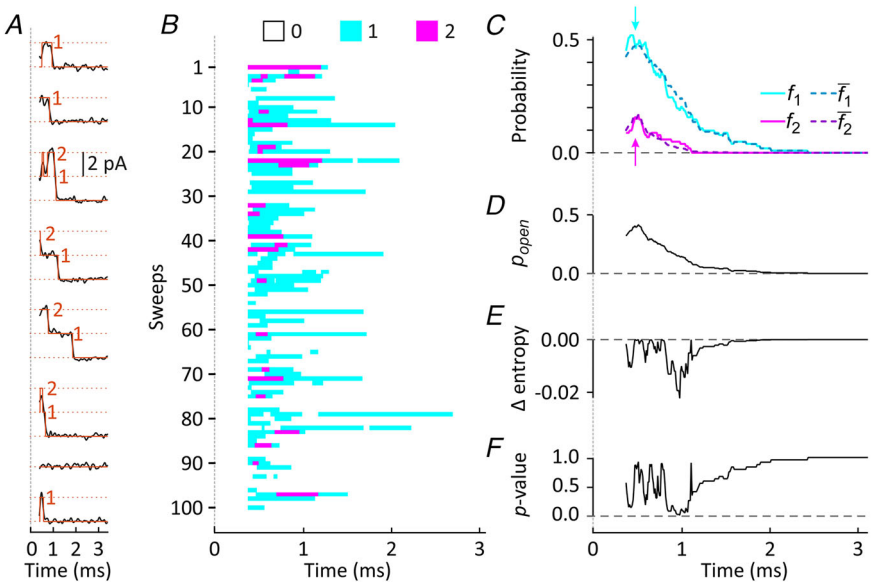

Figure 4. Analysis of $Na_v1.5$ channel interactions in an isolated murine ventricular myocyte patch
A, example sweeps (black, de-trended and filtered) recorded from a murine ventricular myocyte patch with two Na^+ channels depolarized (at time 0) to −40 mV, together with the idealized current (orange). *B*, colour map representation of 100 successfully recorded sweeps. *C*, observed fractions of sweeps with one and two open channels and expected fractions based on the binomial distribution. Arrows highlight that f_1 (cyan) is similar to $\overline{f_1}$ (sea blue) and f_2 (magenta) is similar to $\overline{f_2}$ (purple). *D*, single-channel open probability. *E*, entropy difference between the distributions. *F*, *p*-value of the χ^2 test comparing the expected and observed distributions. Same layout as in Fig. 3.

the distributions remained small (Fig. 5*E*), between 0 and −0.015, and the duration of the longest segment with $p < 0.05$ for the χ^2 test was 0.20 ms (Fig. 5*F*). Thus, there was no manifest functional interaction between the channels.

Figure 6 illustrates that our analysis can also applied to more than two channels. In Fig. 6, an HEK cell patch with four human $Na_v1.5$ channels was examined. The protocol yielded 516 utilizable sweeps (Fig. 6*A*) before the seal was lost. Figure 6*B* shows the proportion of sweeps that exhibited one to four open channels *vs.* time (f_1 to f_4) and the corresponding proportions based on the binomial distribution ($\overline{f_1}$ to $\overline{f_4}$). In the presence of more than two channels, the interpretation of these distributions is slightly different from that with only two channels. Under the hypothesis of cooperative gating, we now anticipate finding $f_1 < \overline{f_1}$ and $f_4 > \overline{f_4}$, while no clear anticipation can be made for f_2 and f_3. The data of Figs 6*B* and 6*C* indeed show that f_1 was less than $\overline{f_1}$ around the peak of p_{open} ($\varepsilon_1 = -0.04$), while f_4 was then more than $\overline{f_4}$ ($\varepsilon_4 = 1.28$). Moreover, f_3 was also larger than the expectation ($\varepsilon_3 = 0.22$), while f_2 was slightly smaller ($\varepsilon_2 = -0.06$). Thus, the fraction of observations with three or four open channels was larger and the fraction with one or two open channels was smaller than the expectation from the binomial distribution. Therefore, there was some synergy between the channels. However, the entropy difference again remained between 0 and −0.015 (Fig. 6*D*), and the duration of the longest segment with $p < 0.05$ for the χ^2 test was only 0.40 ms, during early inactivation (Fig. 6*E*).

Table 1 lists all 16 experiments in which at least 100 sweeps were recorded successfully. The durations of the longest segments with $p < 0.05$ ranged from 0 to 0.45 ms, and these segments occurred inconsistently during diverse phases (activation, near the peak, inactivation) of the ensemble average current. The brevity of such segments and their inconsistent occurrence thus do not lend support to the idea that Na^+ channels interact functionally. Furthermore, ε_1, expected to be negative in the presence of cooperative openings, was positive in some experiments. In addition, ε_1 in our experiments was considerably closer to 0 compared to $\varepsilon_1 = -0.69$, the value we calculated previously based on the data of (Clatot et al., 2017; Hichri et al., 2020). Considering all the experiments listed in Table 1, ε_1 was 0.018 ± 0.051 (mean ± SD) and was not statistically different from 0 ($P = 0.1768$, two-tailed Student's *t* test *vs.* 0; $P = 0.3255$, Wilcoxon signed rank test). This suggests that under

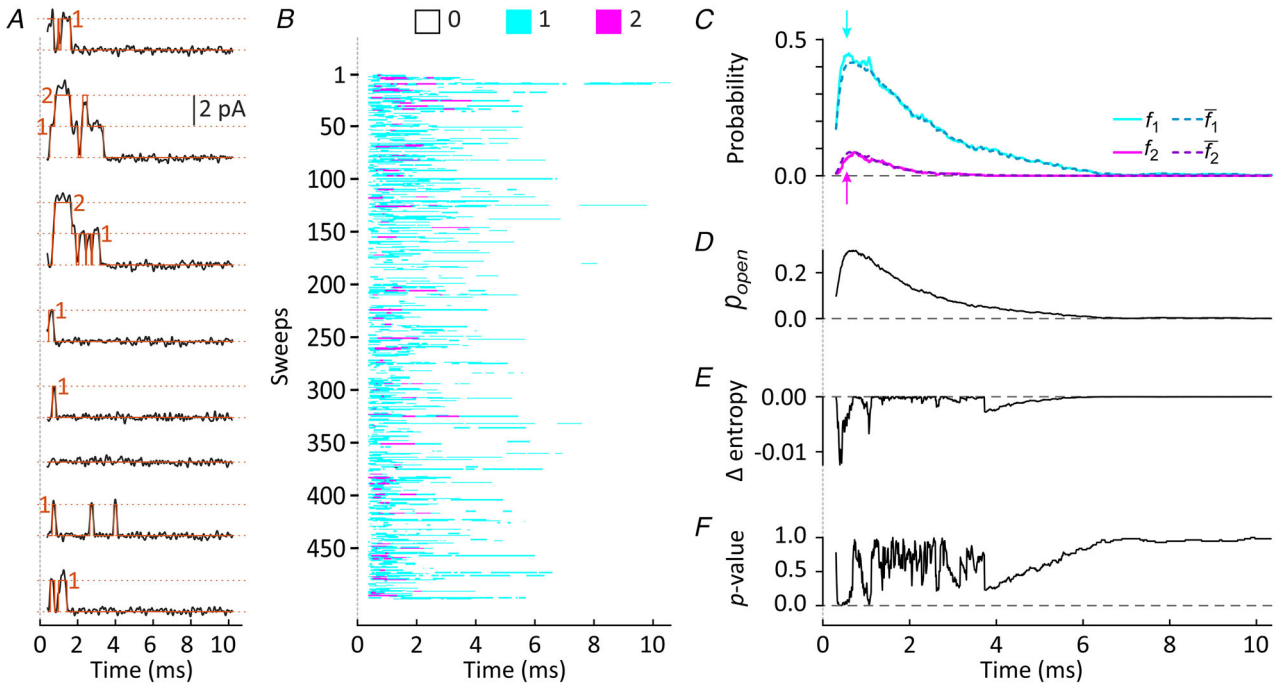

Figure 5. Analysis of $Na_v1.5$ channel interactions in an isolated rabbit ventricular myocyte patch
A, example sweeps (black, de-trended and filtered) recorded from a rabbit ventricular myocyte patch with two Na^+ channels depolarized (at time 0) to −60 mV, together with the idealized current (orange). *B*, colour map representation of 498 successful sweeps. *C*, observed fractions of sweeps with one and two open channels and expected fractions based on the binomial distribution. Arrows indicate the smaller f_1 (cyan) relative to $\overline{f_1}$ (sea blue) and the larger f_2 (magenta) relative to $\overline{f_2}$ (purple). *D*, single-channel open probability. *E*, entropy difference between the distributions. *F*, *p*-value of the χ^2 test comparing the expected and observed distributions. Same layout as in Figs 3 and 4.

Table 1. Summary of experiments.

Cell type, species	Experimental index	Voltage step (mV)	Number of sweeps, N_{sweeps}	Number of channels, $N_{assumed}$	Peak of p_{open}	Values of ε_k				χ^2 test: longest segment and phase	
						ε_1	ε_2	ε_3	ε_4	Longest segment (ms) with $p < 0.05$	Phase of occurrence
HEK293/hNa$_v$1.5	Cell 01	+40	100	2	0.31	−0.03	0.09			0.04	During activation
HEK293/hNa$_v$1.5	Cell 01	+60	160	2	0.16	0.11	−0.72			0.13	Around peak
HEK293/hNa$_v$1.5	Cell 02	+40	100	3	0.11	0.03	−0.24	1.76		0.17	During activation
HEK293/hNa$_v$1.5	Cell 02	+60	100	3	0.06	0.02	−0.13	−1.00		0.00	
HEK293/hNa$_v$1.5	Cell 03	+60	100	3	0.21	0.08	−0.02	−0.03		0.07	During activation
HEK293/hNa$_v$1.5	Cell 04	+60	250	4	0.17	−0.02	−0.07	0.33	3.47	0.45	Early inactivation
HEK293/hNa$_v$1.5	Cell 05	+40	516	4	0.26	−0.04	−0.06	0.22	1.28	0.40	Early inactivation
HEK293/hNa$_v$1.5	Cell 06	+60	500	3	0.10	0.02	−0.08	0.15		0.27	Late inactivation
HEK293/hNa$_v$1.5	Cell 07	+60	500	3	0.10	−0.05	0.23	0.75		0.38	Early inactivation
HEK293/hNa$_v$1.5	Cell 08	+40	1000	3	0.08	0.01	−0.05	−0.54		0.07	Late inactivation
HEK293/hNa$_v$1.5	Cell 09	+40	100	4	0.14	−0.03	0.02	0.38	−1	0.09	Early inactivation
Mouse CM	Cell 01	+60	398	3	0.11	0.12	−0.49	−0.68		0.09	Late inactivation
Mouse CM	Cell 07	+40	100	2	0.43	−0.01	0.02			0.06	Late inactivation
Mouse CM	Cell 10	+40	200	4	0.10	0.00	−0.43	−1		0.1	Late inactivation
Rabbit CM	Cell 01	+60	498	2	0.30	0.05	−0.01			0.20	During activation
Rabbit CM	Cell 02	+60	350	3	0.20	0.03	−0.02	−0.33		0.30	Late inactivation

CM: ventricular cardiomyocyte; hNa$_v$1.5: expressing human Na$_v$1.5 channels. Figure 3 shows results with HEK293/hNa$_v$1.5 cell 01 at +40 mV. Figure 4 shows results with mouse cell 07 at +40 mV. Figures 5 and 8 show results with rabbit cell 01 at +60 mV. Figure 6 shows results with HEK293/hNa$_v$1.5 cell 05 at +40 mV.

our experimental conditions, the cooperative interaction between channels was very weak, if present at all.

Single-channel conductances are typical of voltage-gated Na^+ channels

Figure 7 shows single $Na_v1.5$ channel current–voltage relationships observed for the HEK cell human $Na_v1.5$ expression system as well as for the adult murine and rabbit ventricular myocytes. For this analysis, protocols with at least 50 sweeps were used and the single-channel current was obtained using our idealization algorithm. On average, single-channel conductance was comparable for all three species (human: 21.9 pS; mouse: 18.8 pS; rabbit: 23.8 pS) and in the range of values reported in the literature (Benndorf, 1994; Kang et al., 2021; van Bemmelen et al., 2004). These values, together with the clearly positive reversal potentials and the typical activation and inactivation time courses of the ensemble average currents (Figs 2–6), demonstrate that our single-channel recordings were indeed carried by voltage-gated Na^+ channels.

Analysis in the time domain does not reveal coupled gating

The analyses presented so far have examined the distributions of the numbers of simultaneously open channels at individual time points, but provide no information with respect to the question of whether

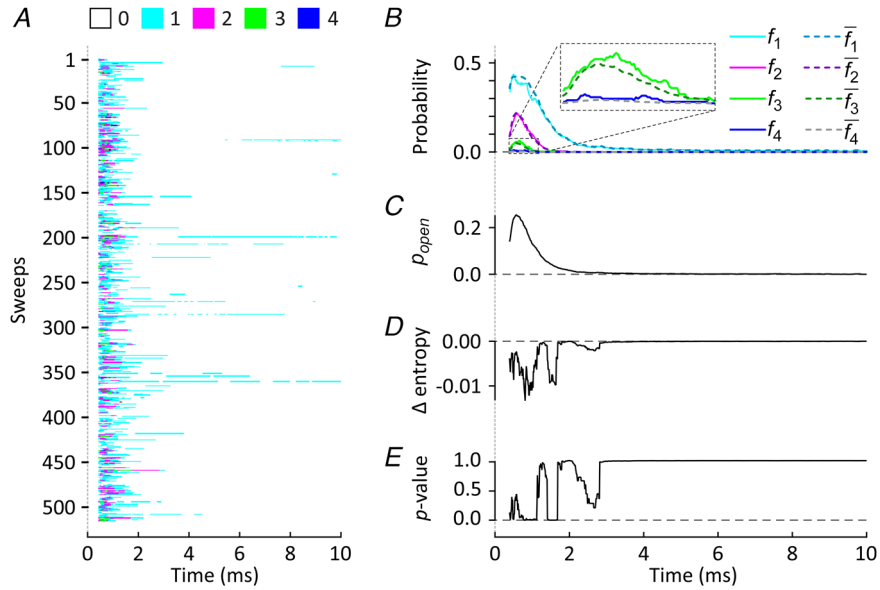

Figure 6. Analysis of interactions between four $hNa_v1.5$ channels in an HEK cell patch based on the expected binomial distribution
The patch was depolarized to −60 mV. *A*, colour map representation of 516 idealized consecutive sweeps. *B*, top plot and inset: observed fractions of sweeps (continuous traces) with one (f_1, cyan), two (f_2, magenta), three (f_3, light green) and four (f_4, dark blue) open channels, and expected fractions (binomial distribution) without interaction [$\overline{f_1}$ (sea blue), $\overline{f_2}$ (purple), $\overline{f_3}$ (dark green) and $\overline{f_4}$ (grey), dotted traces of corresponding colours]. *C*, single-channel open probability. *D*, entropy difference between the observed and expected distributions. *E*, *p*-value of the χ^2 test comparing the expected and observed distributions.

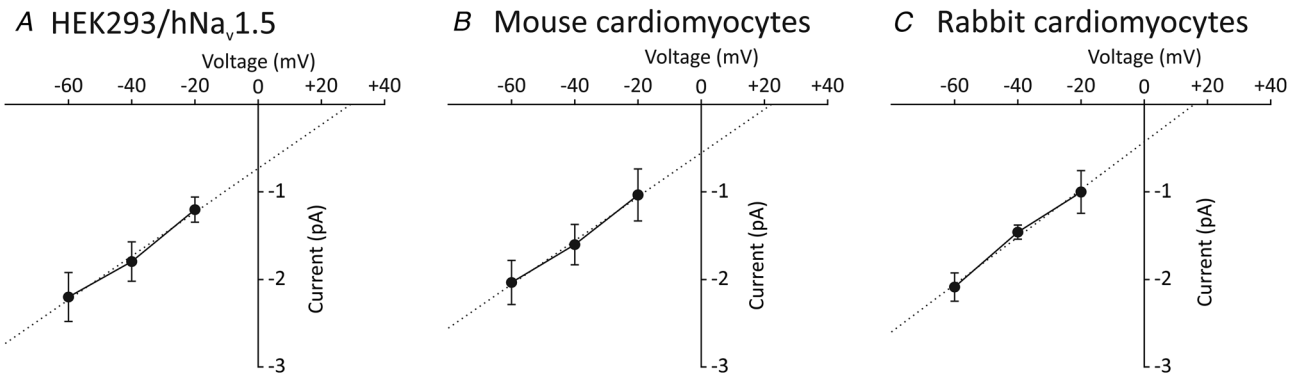

Figure 7. Single $Na_v1.5$ channel current–voltage relationships and single-channel conductances
Single-channel current–voltage relationships and regression lines (dotted) in cell-attached patches from: *A*, HEK cells expressing human $Na_v1.5$ channels (n = 4); *B*, adult murine ventricular myocytes (n = 4); and *C*, adult rabbit ventricular myocytes (n = 2). The voltage axes represent the negative of the applied potential, corresponding to transmembrane potential under the assumption that the elevated extracellular K^+ concentration (140 mmol/L) depolarized the cells to 0 mV. The currents, being inward, are represented with a negative sign according to the usual convention. Data points and error bars show mean ± SD.

channel openings or closings occur close together in time. To answer this question and further substantiate the absence of coupled gating in our experiments, we developed an analysis based on the approach by Chung and Kennedy (1996). First, we estimated the probabilities of transiting from a configuration with i open channels to one with j open channels ($r_{i\to j}$) between a given time t_1 and time $t_2 = t_1 + \Delta t$, with a fixed Δt and with t_1 sliding along the depolarizing step. Then, we compared these probabilities with those expected according to Chung and Kennedy assuming identical, indistinguishable and independent (non-interacting) channels. As time interval Δt, we used 0.05 ms (five samples). This is approximately the time constant of the low-pass filter used. Of note, this analysis requires a sufficient number of sweeps (>400) to provide a meaningful result, and we illustrate it in Fig. 8 for the 498 sweeps recorded from a rabbit cardiomyocyte patch with two Na^+ channels (same data as in Fig. 5*B*).

Figure 8 shows that the transition probability $r_{0\to 2}$ of going from zero to two open channels within the interval Δt was not larger (in fact lower) than expected for independent channels, arguing against the idea of coupled openings. Similarly, $r_{2\to 0}$ was not larger either (in fact lower) than expected for independent channels, arguing against the suggestion of coupled closings. Thus, the results of this analysis contradict the hypothesis of coupled gating. Similar results were obtained for a Δt of 0.1 and 0.2 ms.

As positive control for the analysis illustrated in Fig. 8, we used data generated by stochastic simulations using our previously published Markovian model of two interacting Na^+ channels (Hichri et al., 2020). In this modelling approach, individual channels were represented by the six-state model of Clancy and Rudy (1999) and a 36-state model of a channel pair was constructed by combining every possible state of the first channel with every possible state of the second. Interactions were then represented by modifying the free energies of the combined states and the energy barriers between these states to mimic the published results of Clatot et al. (2017). Specifically, the interaction (called Interaction II in Hichri et al., 2020) produced a strongly increased f_2, a strongly decreased f_1 as well as coupled openings and closings (the majority of latencies between coupled openings/closings within 0.01 ms), without a manifest difference in ensemble average current.

Figure 9 shows that the observed $r_{0\to 2}$ was clearly larger than that expected for independent channels up to 1 ms (activation phase), reflecting the coupled openings, while the observed $r_{2\to 0}$ was larger than that expected up to 1.5 ms (inactivation), reflecting the coupled closings. Furthermore, $r_{1\to 0}$ and $r_{1\to 2}$ were also increased, indicating that the situation with only one open channel is less stable. Moreover, $r_{0\to 1}$, $r_{1\to 1}$ and $r_{2\to 1}$ were all decreased, reflecting the fact that the system of two channels was less prone to transition into a configuration with one open channel, again suggesting coupled gating.

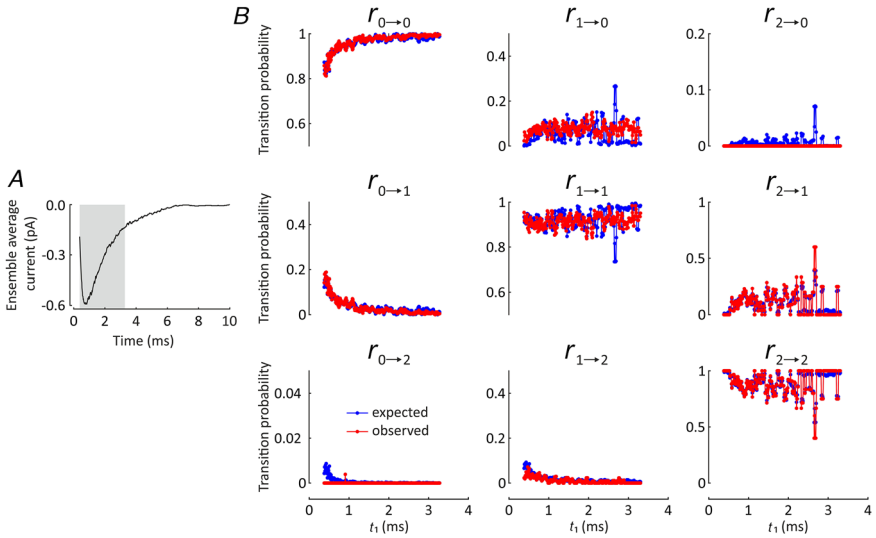

Figure 8. Analysis of coupled gating between two Na^+ channels in a rabbit ventricular myocyte patch
This analysis was conducted on the same set of 498 sweeps with voltage step to −60 mV shown in Fig. 5*B*. *A*, ensemble average current; the grey rectangle corresponds to the interval analysed in *B*. *B*, the individual panels (labels) show the estimated transition probabilities $r_{i\to j}$ of going from a configuration with i open channels to one with j open channels between time t_1 (after the onset of the voltage step, abscissae) and time $t_2 = t_1 + \Delta t$, with $\Delta t = 0.05$ ms. Red data points show the probabilities estimated directly from the data and blue data points show the expected probabilities under the assumption that the channels are independent, calculated according to Chung and Kennedy (1996).

This positive control analysis underlines the idea that coupled gating was absent in the experiment in Fig. 8, or that the two channels were even prevented from opening or closing together. Our results also demonstrate that the analysis of Chung and Kennedy can be used for non-stationary single-channel recordings.

Discussion

In this work, we have developed a novel automatic pipeline to de-trend and analyse single-channel currents from cell-attached patch-clamp recordings with the aim to quantify functional channel–channel interactions. We performed cell-attached recordings of Na^+ currents, not only in HEK293 cells expressing wild-type human $Na_v1.5$ channels but also in adult mouse and rabbit cardiomyocytes. The latter cells permitted us to assess the presence or absence of interactions between $Na_v1.5$ channels from other species in their native cellular environment.

In contrast to the findings of Clatot et al. (2017) that voltage-gated Na^+ channels exhibit cooperative and coupled gating, we did not uncover any quantitative evidence of such interactions in our recordings, neither in the same HEK293 cell expression system nor in isolated cardiomyocytes. Indeed, the time intervals consistent with cooperativity with $p < 0.05$ (repeated χ^2 test) when comparing the observed distributions of current levels *vs*. the expected binomial distributions were too brief and occurred inconsistently during different phases of the ensemble average current. Moreover, when comparing these distributions, we observed that the relative difference for the first level at the moment of peak p_{open} (our quantitative parameter ε_1) was in most experiments positive or very close to 0, and, on average, not clearly different from 0. This observation does not support the hypothesis of cooperative gating, which is expected to decrease the probability of observing only one open channel. In experiments with two channels, the relative difference for the second level (ε_2) was frequently negative, which also does not support this hypothesis. Furthermore, our refined analysis based on the method of Chung and Kennedy (1996) did not demonstrate any increased propensity of the channels synchronizing their openings and closings. Together, under our experimental conditions, we do not corroborate the presence of coupled gating between $Na_v1.5$ channels.

Our results are sustained by several methodological and technical advantages. First, we did not limit our experiments and analysis only to patches containing two channels, because if channels do interact, this interaction would also have been revealed by our parameter ε_1 in the case of three or more channels. Second, all the currents were recorded at a sampling frequency of 100 kHz with only minimal filtering, which allowed us to have a high temporal resolution and thus more accuracy in the analysis. Third, we aimed to obtain large numbers of sweeps in individual patches and did not pool sweeps

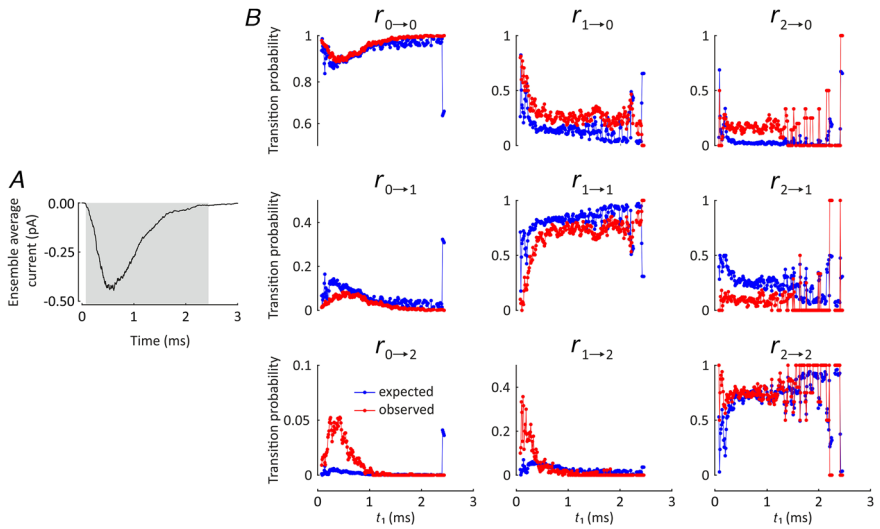

Figure 9. Analysis of coupled gating in a Markovian model of two interacting Na^+ channels
The same analysis as in Fig. 8 was conducted for a stochastic simulation (1000 sweeps) of a pair of interacting Markovian cardiac Na^+ channel models with coupled gating (Hichri et al., 2020). The voltage was stepped to −20 mV at time 0. *A*, ensemble average current; the grey rectangle corresponds to the interval analysed in *B*. *B*, the individual panels (labels) show the estimated transition probabilities $r_{i\to j}$ of going from a configuration with i open channels to one with j open channels between time t_1 (abscissae) and $t_2 = t_1 + \Delta t$, with $\Delta t = 0.05$ ms. Red: probabilities estimated directly from the simulated data. Blue: expected probabilities under the assumption of channel independence.

from different patches. Because different patches may be intrinsically dissimilar due to cellular variability, we thereby avoided possible confounding factors arising from such pooling. Finally and importantly, all our cell-attached recordings were processed and idealized with the same automated pipeline and with a minimal number of manual settings. One strength of our idealization algorithm is that it considers the entire set of sweeps simultaneously rather than sequentially sweep by sweep.

The question thus arises why our results are different from those of Clatot et al. (2017). One possible explanation is that the experimental conditions (including culture conditions), although comparable, were not identical. In particular, we opted for a physiological Na^+ concentration (140 mmol/L) in the pipette, while Clatot et al. (2017) used an increased Na^+ concentration of 280 mmol/L. The resulting difference in osmolarity may possibly have caused the channels to interact in their experiments. Another possible explanation is that wild-type Na^+ channels only very rarely form functionally interacting pairs and we were unfortunate to miss this phenomenon in our entire set of experiments. If such interactions are indeed very rare (in the wild-type situation), it is then questionable whether it modifies cardiac cellular excitability in a substantial and relevant manner.

Comparison to previous studies

The question of whether Na^+ channels functionally interact has been a matter of debate since the 1980s. While performing cell-attached and inside out patch-clamp recordings with a neuroblastoma cell line, Aldrich et al. (1983) observed that there was a higher probability of an even number of channels under the pipette than an odd number, which led to the suggestion that Na^+ channels might not be independent entities. However, by analysing the mean durations of periods with only one channel open *vs*. two channels open simultaneously, they later did not detect any difference between the observed mean periods with two open channels and the predicted mean periods based on the open lifetime of a single channel under the assumption of independent channels (Aldrich & Stevens, 1987). This led them to conclude that there is no inter-channel cooperativity. Kiss and Nagy (1985) also addressed the question of whether Na^+ channels interact by performing cell-attached recordings in mouse neuroblastoma cells. They reported that in their recordings, there was a tendency of blank sweeps (without any channel activity) and of sweeps with channel openings (irrespective of whether one, two or more channels opened) to form clusters of consecutive sweeps (Kiss & Nagy, 1985). In patches with three or more channels recorded at positive transmembrane potentials ($>$10 mV), they demonstrated that sweeps with channel openings tend to form large clusters. However, this finding can be explained by the larger channel open probability at potentials $>$10 mV (Kiss & Nagy, 1985). In a computational model, Naundorf et al. (2006) showed that by introducing populations of coupled Na^+ channels, it was possible to replicate the rapid initiation and variable onset voltage of neuronal action potentials as seen in experiments. However, they did not perform any single-channel recordings to quantify or substantiate this coupling.

Although we did not observe functional channel–channel interactions, our results do not exclude the idea that Na^+ channels can form dimers or multimers (biochemical interaction) as reported in previous studies (Clatot et al., 2017; Iamshanova et al., 2022). Our results also do not exclude the possibility that channels start interacting under conditions of cellular stress. For example, Undrovinas et al. (1992) showed that during voltage steps starting from a very negative holding potential (≤ -150 mV) and in the presence of the ischaemic metabolite lysophosphatidylcholine, cardiac Na^+ channels tend to exhibit synchronized openings and closings. However, the proportion of patches with channels exhibiting coupled gating was low, in the range of a few per cent. Intriguingly, there are also reports that Na^+ channels may exhibit negative cooperativity. For example, in experiments with batrachotoxin-modified neuronal channels, Iwasa et al. (1986) observed that the likelihood of having two channels open together was lower than that expected from the binomial distribution. Conversely, the probability of having only one channel open was higher than the expected one (corresponding to a positive ε_1 in our framework). All these effects reported under stress conditions may be the consequence of a direct interaction between channels, or an indirect one consecutive to modifications in the regulatory proteins of the Na^+ channel complex.

Clinical implications and translational perspective

While our results do not provide evidence of functional interactions between wild-type $Na_v1.5$ channels, they do not exclude that Na^+ channel variants may possibly exhibit functional interactions between themselves or with wild-type channels. This may be relevant in the context of inherited channelopathies when typically variant and wild-type channels are co-expressed (Clatot et al., 2018; Ruhlmann et al., 2020; Sottas & Abriel, 2016). Furthermore, a functional interaction may be caused and modulated by a vast array of Na^+ channel-associated proteins under specific conditions not met under our experimental conditions. Our analysis pipeline offers the prospect to process single/multi-channel recordings with minimal human interventions, and the output idealized

current can then be used to explore potential cooperativity in variant dimers and multimers of $Na_v1.5$ channels as well as in other channels from the $Na_v1.X$ family. If such interactions are identified and if they appear relevant for function, this can pave new ways for the discovery of new therapeutic targets for arrhythmias and neurological disorders.

Limitations

Despite the rigor of our analysis, our work has several limitations that should be discussed. First, our analyses require a large number of sweeps (at least 100, but ideally 1000 or more) to have sufficient power. However, this is inherent to any method examining interactions at the single-channel level due to the stochastic nature of channel gating. Obtaining large numbers of sweeps from the same patch is challenging and frequently limited by the instability of the patch and its seal. Second, performing cell-attached recordings may be associated with the difficulty of controlling transmembrane potential precisely. Thus, experiments conducted with the same test potential but on different cells may lead to different peak open probabilities, and thus such experiments cannot be directly compared. This was the principal reason why we did not pool sets of sweeps in our analyses. A possible solution would be to use excised inside-out or outside-out patches, but this will occur at the expense of losing the intracellular environment on the intracellular side of the channels, especially the biochemical interaction of the $Na_v1.5$ channels with intracellular anchoring or regulatory proteins (Allouis et al., 2006; Gavillet et al., 2006; Jespersen et al., 2006; Kang et al., 2021; Lemaillet et al., 2003). This aspect is particularly important when one investigates the gating behaviour of the channels in isolated cardiomyocytes. However, excised patches may be less stable than cell-attached recordings.

Because Na^+ channels activate and inactivate faster at large depolarizing step potentials, we limited our cell-attached recordings to low depolarizing steps between −60 and −20 mV. This was necessary, because at more positive step potentials, a large number of channel openings are completely masked by the capacitive artefact and the de-trending algorithm no longer operates reliably. Moreover, single-channel current amplitudes become smaller with increasing step voltages (see Fig. 7), which also affects the reliability of the idealization procedure. Thus, one may argue that cooperative gating could be more apparent at higher voltages. At such voltages, the openings may merge more due to shorter latencies to first opening and shorter open times, which may then give a false impression of cooperative gating. This underlies the importance of always applying a rigorous unbiased analysis.

Another important point to note is that one does not know the true number of channels in a patch. It can never be excluded that in a given patch there were more channels than the maximal number of simultaneously open channels observed in the corresponding set of sweeps, raising the question of how underestimating the number of assumed channels $N_{assumed}$ would affect the results. To answer this question, we repeated the analyses in Figs 3–6 and Table 1 with increasing values of $N_{assumed}$. Interestingly, increasing $N_{assumed}$ by one, two or three channels always increased the values of ε_1, which became more and more positive. Since ε_1 is, in our opinion, a suitable marker to ascertain the magnitude of the effect of any putative interaction, these tests do not support the idea that underestimating the true number of channels may have concealed cooperative or coupled gating in our analysis. Moreover, increasing $N_{assumed}$ had only a minor influence on the calculated intervals during which the p-values of the χ^2 tests were <0.05.

It may be speculated that cooperative interactions appear only in the presence of larger numbers or densities of Na^+ channels, as suggested and modelled mathematically in a neuroscience study by Naundorf et al. (2006). The performance of our idealization algorithm decreases with increasing channel numbers because of the additional noise arising from the intrinsic fluctuations of the current flowing through open channels, which blurs the individual current levels. Evidencing interactions at the single-channel levels is therefore difficult in the presence of larger Na^+ channel clusters. In this context, further insight may be provided by non-stationary mean-variance analysis (Hille, 2001; Sigworth, 1980), an elegant technique in which the relationship between the variance and the mean of the current is fitted by the quadratic function predicted by the binomial distribution expected for independent channels. The single-channel current is then obtained from the initial slope of the quadratic relationship. However, if channels gate cooperatively, this technique will overestimate the single-channel current. For example, if channel clusters consist of dimers that open and close almost together, then the single-channel current would be overestimated by a factor close to 2. Because we did not find substantial functional interactions in the first place, we did not pursue this aspect further.

Finally, in the absence of any experimental positive control data, we had recourse to computer simulations of interacting channels (Fig. 9).

Conclusions

Whether cardiac Na^+ channels or channels of the $Na_v1.X$ family interact functionally is controversial, and our study will not resolve the debate. However, our

study underlines the value of recording as many sweeps as possible to address this question. It also underlines the importance of rigorous and unbiased signal processing and the development and application of appropriate analyses. We believe that continuing research on this controversial question is nevertheless necessary, as discovering situations in which channels do interact may have a profound impact on fundamental notions of physiology with outreaching consequences for biomedical applications.

References

Abrams, J., Roybal, D., Chakouri, N., Katchman, A. N., Weinberg, R., Yang, L., Chen, B. X., Zakharov, S. I., Hennessey, J. A., Avula, U. M. R., Diaz, J., Wang, C., Wan, E. Y., Pitt, G. S., Ben-Johny, M., & Marx, S. O. (2020). Fibroblast growth factor homologous factors tune arrhythmogenic late $Na_v1.5$ current in calmodulin binding-deficient channels. *JCI Insight*, **5**(19), e141736.

Abriel, H., Rougier, J. S., & Jalife, J. (2015). Ion channel macromolecular complexes in cardiomyocytes: Roles in sudden cardiac death. *Circulation Research*, **116**(12), 1971–1988.

Ahern, C. A., Payandeh, J., Bosmans, F., & Chanda, B. (2016). The hitchhiker's guide to the voltage-gated sodium channel galaxy. *Journal of General Physiology*, **147**(1), 1–24.

Aldrich, R. W., Corey, D. P., & Stevens, C. F. (1983). A reinterpretation of mammalian sodium channel gating based on single channel recording. *Nature*, **306**(5942), 436–441.

Aldrich, R. W., & Stevens, C. F. (1987). Voltage-dependent gating of single sodium channels from mammalian neuroblastoma cells. *Journal of Neuroscience*, **7**(2), 418–431.

Allouis, M., Le Bouffant, F., Wilders, R., Peroz, D., Schott, J. J., Noireaud, J., Le Marec, H., Merot, J., Escande, D., & Baro, I. (2006). 14-3-3 is a regulator of the cardiac voltage-gated sodium channel $Na_v1.5$. *Circulation Research*, **98**(12), 1538–1546.

Benndorf, K. (1994). Properties of single cardiac Na^+ channels at 35 degrees C. *Journal of General Physiology*, **104**(5), 801–820.

Bezzina, C. R., Rook, M. B., Groenewegen, W. A., Herfst, L. J., van der Wal, A. C., Lam, J., Jongsma, H. J., Wilde, A. A., & Mannens, M. M. (2003). Compound heterozygosity for mutations (W156X and R225W) in SCN5A associated with severe cardiac conduction disturbances and degenerative changes in the conduction system. *Circulation Research*, **92**(2), 159–168.

Boixel, C., Gavillet, B., Rougier, J. S., & Abriel, H. (2006). Aldosterone increases voltage-gated sodium current in ventricular myocytes. *American Journal of Physiology. Heart and Circulatory Physiology*, **290**(6), H2257–H2266.

Chung, S. H., & Kennedy, R. A. (1996). Coupled Markov chain model: Characterization of membrane channel currents with multiple conductance sublevels as partially coupled elementary pores. *Mathematical Biosciences*, **133**(2), 111–137.

Clancy, C. E., & Rudy, Y. (1999). Linking a genetic defect to its cellular phenotype in a cardiac arrhythmia. *Nature*, **400**(6744), 566–569.

Clatot, J., Hoshi, M., Wan, X., Liu, H., Jain, A., Shinlapawittayatorn, K., Marionneau, C., Ficker, E., Ha, T., & Deschenes, I. (2017). Voltage-gated sodium channels assemble and gate as dimers. *Nature Communications*, **8**(1), 2077.

Clatot, J., Zheng, Y., Girardeau, A., Liu, H., Laurita, K. R., Marionneau, C., & Deschenes, I. (2018). Mutant voltage-gated Na^+ channels can exert a dominant negative effect through coupled gating. *American Journal of Physiology. Heart and Circulatory Physiology*, **315**(5), H1250–H1257.

Dong, C., Wang, Y., Ma, A., & Wang, T. (2020). Life cycle of the cardiac voltage-gated sodium channel $Na_v1.5$. *Frontiers in Physiology*, **11**, 609733.

Gavillet, B., Rougier, J. S., Domenighetti, A. A., Behar, R., Boixel, C., Ruchat, P., Lehr, H. A., Pedrazzini, T., & Abriel, H. (2006). Cardiac sodium channel $Na_v1.5$ is regulated by a multiprotein complex composed of syntrophins and dystrophin. *Circulation Research*, **99**(4), 407–414.

Grundy, D. (2015). Principles and standards for reporting animal experiments in The Journal of Physiology and Experimental Physiology. *The Journal of Physiology*, **593**(12), 2547–2549.

Hichri, E., Selimi, Z., & Kucera, J. P. (2020). Modeling the interactions between sodium channels provides insight into the negative dominance of certain channel mutations. *Frontiers in Physiology*, **11**, 589386.

Hille, B. (2001). *Ionic Channels of Excitable Membranes*. Sinauer Associates Inc., Sunderland.

Iamshanova, O., Hämmerli, A.-F., Ramaye, E., Seljmani, A., Ross-Kaschitza, D., Schärz, N., Essers, M., Guichard, S., Rougier, J.-S., & Abriel, H. (2022). Role of 14-3-3 proteins in human cardiac sodium channel $Na_v1.5$ regulation. *BioRxiv*. https://doi.org/10.1101/2022.10.26.513875.

Iwasa, K., Ehrenstein, G., Moran, N., & Jia, M. (1986). Evidence for interactions between batrachotoxin-modified channels in hybrid neuroblastoma cells. *Biophysical Journal*, **50**(3), 531–537.

Jespersen, T., Gavillet, B., van Bemmelen, M. X., Cordonier, S., Thomas, M. A., Staub, O., & Abriel, H. (2006). Cardiac sodium channel $Na_v1.5$ interacts with and is regulated by the protein tyrosine phosphatase PTPH1. *Biochemical and Biophysical Research Communications*, **348**(4), 1455–1462.

Kang, P. W., Chakouri, N., Diaz, J., Tomaselli, G. F., Yue, D. T., & Ben-Johny, M. (2021). Elementary mechanisms of calmodulin regulation of $Na_v1.5$ producing divergent arrhythmogenic phenotypes. *PNAS*, **118**(21), e2025085118.

Kim, J., Ghosh, S., Liu, H., Tateyama, M., Kass, R. S., & Pitt, G. S. (2004). Calmodulin mediates Ca^{2+} sensitivity of sodium channels. *Journal of Biological Chemistry*, **279**(43), 45004–45012.

Kiss, T., & Nagy, K. (1985). Interaction between sodium channels in mouse neuroblastoma cells. *European Biophysics Journal*, **12**(1), 13–18.

Kléber, A. G., & Rudy, Y. (2004). Basic mechanisms of cardiac impulse propagation and associated arrhythmias. *Physiological Reviews*, **84**(2), 431–488.
Lemaillet, G., Walker, B., & Lambert, S. (2003). Identification of a conserved ankyrin-binding motif in the family of sodium channel alpha subunits. *Journal of Biological Chemistry*, **278**(30), 27333–27339.
Lieve, K. V., & Wilde, A. A. (2015). Inherited ion channel diseases: A brief review. *Europace*, **17**(Suppl 2), ii1–ii6.
McNair, W. P., Ku, L., Taylor, M. R., Fain, P. R., Dao, D., Wolfel, E., & Mestroni, L., Familial Cardiomyopathy Registry Research G. (2004). SCN5A mutation associated with dilated cardiomyopathy, conduction disorder, and arrhythmia. *Circulation*, **110**(15), 2163–2167.
Naundorf, B., Wolf, F., & Volgushev, M. (2006). Unique features of action potential initiation in cortical neurons. *Nature*, **440**(7087), 1060–1063.
Nelder, J. A., & Mead, R. (1965). A simplex method for function minimization. *The Computer Journal*, **7**(4), 308–313.
Odening, K. E., Bodi, I., Franke, G., Rieke, R., Ryan de Medeiros, A., Perez-Feliz, S., Furniss, H., Mettke, L., Michaelides, K., Lang, C. N., Steinfurt, J., Pantulu, N. D., Ziupa, D., Menza, M., Zehender, M., Bugger, H., Peyronnet, R., Behrends, J. C., Doleschall, Z., … Brunner, M. (2019). Transgenic short-QT syndrome 1 rabbits mimic the human disease phenotype with QT/action potential duration shortening in the atria and ventricles and increased ventricular tachycardia/ventricular fibrillation inducibility. *European Heart Journal*, **40**(10), 842–853.
Olson, T. M., & Keating, M. T. (1996). Mapping a cardiomyopathy locus to chromosome 3p22-p25. *Journal of Clinical Investigation*, **97**(2), 528–532.
Rivaud, M. R., Delmar, M., & Remme, C. A. (2020). Heritable arrhythmia syndromes associated with abnormal cardiac sodium channel function: Ionic and non-ionic mechanisms. *Cardiovascular Research*, **116**(9), 1557–1570.
Rougier, J. S., Essers, M. C., Gillet, L., Guichard, S., Sonntag, S., Shmerling, D., & Abriel, H. (2019). A distinct pool of $Na_v1.5$ channels at the lateral membrane of murine ventricular cardiomyocytes. *Frontiers in Physiology*, **10**, 834.
Ruan, Y., Liu, N., & Priori, S. G. (2009). Sodium channel mutations and arrhythmias. *Nature Reviews Cardiology*, **6**(5), 337–348.
Ruhlmann, A. H., Korner, J., Hausmann, R., Bebrivenski, N., Neuhof, C., Detro-Dassen, S., Hautvast, P., Benasolo, C. A., Meents, J., Machtens, J. P., Schmalzing, G., & Lampert, A. (2020). Uncoupling sodium channel dimers restores the phenotype of a pain-linked $Na_v1.7$ channel mutation. *British Journal of Pharmacology*, **177**(19), 4481–4496.
Shannon, C. E. (1948). A mathematical theory of communication. *Bell System Technical Journal*, **27**(3), 379–423.
Sigworth, F. J. (1980). The variance of sodium current fluctuations at the node of Ranvier. *The Journal of Physiology*, **307**(1), 97–129.
Sottas, V., & Abriel, H. (2016). Negative-dominance phenomenon with genetic variants of the cardiac sodium channel $Na_v1.5$. *Biochimica Et Biophysica Acta*, **1863**(7), 1791–1798.
Undrovinas, A. I., Fleidervish, I. A., & Makielski, J. C. (1992). Inward sodium current at resting potentials in single cardiac myocytes induced by the ischemic metabolite lysophosphatidylcholine. *Circulation Research*, **71**(5), 1231–1241.
van Bemmelen, M. X., Rougier, J. S., Gavillet, B., Apotheloz, F., Daidie, D., Tateyama, M., Rivolta, I., Thomas, M. A., Kass, R. S., Staub, O., & Abriel, H. (2004). Cardiac voltage-gated sodium channel $Na_v1.5$ is regulated by Nedd4-2 mediated ubiquitination. *Circulation Research*, **95**(3), 284–291.
Veerman, C. C., Wilde, A. A., & Lodder, E. M. (2015). The cardiac sodium channel gene SCN5A and its gene product $Na_v1.5$: Role in physiology and pathophysiology. *Gene*, **573**(2), 177–187.
Wilde, A. A. M., & Amin, A. S. (2018). Clinical spectrum of SCN5A mutations: Long QT syndrome, Brugada syndrome, and cardiomyopathy. *JACC Clinical Electrophysiology*, **4**(5), 569–579.

Additional information

Open research badges

This article has earned an Open Data badge for making publicly available the digitally-shareable data necessary to reproduce the reported results. The data is available at https://doi.org/10.5281/zenodo.7817601.

Data availability statement

Na^+ current recordings as well as the MATLAB code permitting the replication of our analysis are available on the repository Zenodo (https://doi.org/10.5281/zenodo.7817601).

Competing interests

The authors have no competing interests to disclose.

Author contributions

J.P.K. designed the study. Z.S. conducted the experiments. Z.S. and J.P.K. wrote computer code and analysed the data. Z.S. prepared the figures. Z.S., J.-S.R., H.A. and J.P.K. drafted the manuscript. All authors approved the final version of the manuscript, agree to be accountable for all aspects of the work in ensuring that questions related to the accuracy or integrity of any part of the work are appropriately investigated and resolved, and all persons designated as authors qualify for authorship, and all those who qualify for authorship are listed.

Funding

This work was supported by the Swiss National Science Foundation (grant number 310030_184707 to J.P.K. and

310030_184783 to H.A.) and a Swiss Government Excellence Scholarship (scholarship number 2019.0238 to Z.S.).

Acknowledgements

The authors thank Julien Louradour, Miriam Barbieri, Nicolò Alerni and Katja Odening for providing freshly isolated rabbit ventricular myocytes. The authors are greatly indebted to Benjamin Haeffele, Billy Kang and Manu Ben-Johny for sharing their MATLAB code to de-trend the recordings. The authors also thank Oksana Iamshanova for enriching discussions, Sabrina Guichard for the preparation of isolated murine myocytes and Anne-Flore Hämmerli for cell culture support.

Open access funding provided by Universität Bern.

Keywords

cardiac electrophysiology, cell-attached patch clamp, cooperative gating, interactions between channels, signal processing, single-channel recordings, sodium channels

Supporting information

Additional supporting information can be found online in the Supporting Information section at the end of the HTML view of the article. Supporting information files available:

Statistical Summary Document
Peer Review History